

Transient domain-wall networks from spontaneous symmetry breaking: A unified solution to the Hubble tension and nanohertz gravitational waves

Ozan Altıntaş¹

¹*Independent Researcher, Istanbul, Turkey**

(Dated: May 13, 2026)

We present a two-field scalar field theory in which spontaneous symmetry breaking produces a transient domain-wall network. A second field χ dynamically generates a time-dependent vacuum bias $\Delta V(t) = 2gv\chi(t)$. Domain walls form at early times when χ is frozen by Hubble friction, producing a stochastic gravitational-wave background with peak frequency in the nanohertz band, consistent with pulsar timing array observations. At late times, when $H(t) \sim m_\chi$ near matter-radiation equality, χ becomes dynamical, activating the bias and causing the network to decay. The residual energy density $\rho_{\text{DW}} = \sigma H$ modifies the Friedmann equation at $z \sim 1$, producing a percent-level enhancement of the Hubble expansion rate that alleviates the Hubble tension. Gravitational waves are continuously produced during the scaling regime, not at the decay time, which separates the two observational signatures. All parameters are derived from the action with no ad-hoc assumptions. The model contains Λ CDM as the $\sigma \rightarrow 0$ limit and predicts a direct correlation $\Omega_{\text{GW}} \propto (\Delta H/H)^2$, testable with future pulsar timing array and CMB data.

I. INTRODUCTION

The standard cosmological model, Λ CDM, provides an excellent description of a wide range of observational data, including the cosmic microwave background (CMB), baryon acoustic oscillations, and large-scale structure [1]. However, several persistent tensions motivate exploring extensions beyond this minimal framework. The most statistically significant among these is the Hubble tension: a discrepancy between early-Universe determinations of the Hubble constant from CMB measurements, $H_0 \approx 67.4 \text{ km s}^{-1} \text{ Mpc}^{-1}$ [1], and late-time distance ladder measurements yielding $H_0 \approx 73 \text{ km s}^{-1} \text{ Mpc}^{-1}$ [2], with a significance exceeding 5σ [3].

Numerous theoretical proposals have been advanced to address this tension, including early dark energy models [4], interacting dark energy scenarios, and modifications of gravity [5]. While many of these can partially alleviate the tension, they often introduce additional parameters or face tight observational constraints from the CMB and large-scale structure.

An alternative and conceptually distinct possibility involves topological defects formed during symmetry-breaking phase transitions in the early Universe [6, 7]. Domain walls naturally arise when a discrete symmetry is spontaneously broken [8]. Stable domain-wall networks are strongly constrained because their energy density would eventually dominate the Universe [9]. However, if the walls are metastable and decay through a small vacuum bias or curvature-driven collapse, they can play a transient but cosmologically significant role [10, 11].

Recent pulsar timing array (PTA) experiments, includ-

ing NANOGrav [12], EPTA [13], and PPTA [14], have reported evidence for a stochastic gravitational-wave background in the nanohertz frequency range. This signal may originate from astrophysical sources, but it could also be a relic from early-Universe phase transitions or topological defect dynamics. Domain-wall networks are known to produce gravitational waves during their evolution and decay [10, 11, 15, 16].

In this work, we construct a cosmological model where an initially symmetric two-field scalar sector undergoes spontaneous symmetry breaking, generating a transient domain-wall network. Starting from the fundamental action in Eq. (3), with a symmetry-breaking potential that admits a \mathbb{Z}_2 vacuum manifold, we derive the full background dynamics. The key novel ingredient is the introduction of a second scalar field χ that couples linearly to ϕ through a term $g\chi\phi$. This coupling generates a time-dependent vacuum bias $\Delta V(t) = 2gv\chi(t)$ that controls the stability of the domain-wall network.

The dynamics of χ are chosen such that the field remains frozen by Hubble friction at early times, allowing domain walls to form and evolve in the scaling regime. During this epoch, the network continuously produces gravitational waves with a characteristic frequency set by the Hubble scale at emission. At late times, when the Hubble parameter drops below the mass scale m_χ near matter-radiation equality, χ becomes dynamical, activating the bias and causing the network to decay.

We show in Sec. IV that during the metastable scaling regime, the coarse-grained energy density of the network scales as $\rho_{\text{DW}} \propto H$, which introduces a linear correction term in the Friedmann equation. This modification enhances the late-time expansion rate while leaving the early Universe essentially unchanged, thereby alleviating the Hubble tension. A percent-level correction to H_0 is obtained for domain-wall tensions $\sigma \sim (10 \text{ MeV})^3$, corresponding to symmetry-breaking scales $v \sim 10 \text{ MeV}$ for

* bukagi@gmail.com

$\mathcal{O}(1)$ couplings.

The same domain-wall dynamics produce gravitational radiation continuously during the scaling regime, not only at the decay time. As demonstrated in Sec. VII, this feature separates the epoch of gravitational-wave production from the epoch of network decay, allowing the model to simultaneously address both observational puzzles without a time-scale inconsistency. The resulting gravitational-wave background peaks in the nanohertz band with amplitude $\Omega_{\text{GW}} \sim 10^{-9}$ - 10^{-8} , consistent with current PTA observations [12–14].

In Appendix A, we perform a covariant second-order perturbation analysis and demonstrate that isocurvature modes decay exponentially, ensuring consistency with CMB constraints. The model contains Λ CDM as the continuous limit when $v \rightarrow 0$ (and hence $\sigma \rightarrow 0$), and predicts a correlated observational signature: a percent-level shift in H_0 implies a gravitational-wave amplitude $\Omega_{\text{GW}} \sim 10^{-9}$ - 10^{-8} in the nanohertz band, with a spectral shape $\Omega_{\text{GW}} \propto f^3$ at low frequencies and $\propto f^{-1}$ at high frequencies.

The paper is organized as follows. Section II defines the fundamental action and derives the field equations. Section III analyzes the vacuum structure and derives the time-dependent bias. Section IV presents the domain-wall solution and network scaling. Section V describes the dynamics of the χ field and the activation of the bias. Section VI computes the gravitational-wave signal from the scaling network. Section VII demonstrates the separation between gravitational-wave production and late-time cosmological effects. Section VIII presents the modified Friedmann equation and the resolution of the Hubble tension. Section IX delineates the allowed parameter window and the correlation between H_0 shift and GW amplitude. Section X discusses observational constraints from CMB, BBN, and PTA. Section XI provides the physical interpretation, and Sec. XII concludes. Detailed derivations are provided in the appendices.

II. ACTION AND FIELD EQUATIONS

A. Action

We consider Einstein gravity minimally coupled to two real scalar fields. The total action is

$$S = \int d^4x \sqrt{-g} \left[\frac{M_{\text{Pl}}^2}{2} R - \frac{1}{2} g^{\mu\nu} \partial_\mu \phi \partial_\nu \phi - \frac{1}{2} g^{\mu\nu} \partial_\mu \chi \partial_\nu \chi - V(\phi, \chi) \right], \quad (1)$$

where $M_{\text{Pl}} = (8\pi G)^{-1/2}$ is the reduced Planck mass. The scalar potential is chosen to exhibit a \mathbb{Z}_2 symmetry-breaking structure for ϕ while providing a mass and a linear coupling for χ :

$$V(\phi, \chi) = \frac{\lambda}{4} (\phi^2 - v^2)^2 + g\chi\phi + \frac{1}{2} m_\chi^2 \chi^2. \quad (2)$$

The theory possesses a discrete \mathbb{Z}_2 symmetry in the ϕ sector when $g = 0$:

$$\phi \rightarrow -\phi, \quad \chi \rightarrow \chi, \quad (3)$$

which will be spontaneously broken when ϕ acquires a vacuum expectation value. The linear coupling $g\chi\phi$ explicitly breaks the \mathbb{Z}_2 symmetry and generates a time-dependent vacuum bias, as shown in Sec. III.

B. Variation and Einstein Equations

Varying the action (1) with respect to the metric $g^{\mu\nu}$ yields the Einstein equations. Using

$$\delta\sqrt{-g} = -\frac{1}{2}\sqrt{-g}g_{\mu\nu}\delta g^{\mu\nu}, \quad (4)$$

and

$$\delta(g^{\mu\nu}\partial_\mu\phi\partial_\nu\phi) = \partial_\mu\phi\partial_\nu\phi\delta g^{\mu\nu}, \quad (5)$$

we obtain

$$\delta S = \frac{1}{2} \int d^4x \sqrt{-g} [M_{\text{Pl}}^2 G_{\mu\nu} - T_{\mu\nu}] \delta g^{\mu\nu}, \quad (6)$$

where $G_{\mu\nu} = R_{\mu\nu} - \frac{1}{2}Rg_{\mu\nu}$ is the Einstein tensor. The energy-momentum tensor is therefore

$$T_{\mu\nu} = \partial_\mu\phi\partial_\nu\phi + \partial_\mu\chi\partial_\nu\chi - g_{\mu\nu} \left[\frac{1}{2}(\partial\phi)^2 + \frac{1}{2}(\partial\chi)^2 + V \right]. \quad (7)$$

The Einstein equations are

$$G_{\mu\nu} = \frac{1}{M_{\text{Pl}}^2} T_{\mu\nu}. \quad (8)$$

C. Scalar Field Equations

Varying the action with respect to the scalar fields gives their equations of motion. For ϕ ,

$$\frac{\delta S}{\delta\phi} = 0 \quad \Rightarrow \quad \frac{1}{\sqrt{-g}}\partial_\mu(\sqrt{-g}g^{\mu\nu}\partial_\nu\phi) + \frac{\partial V}{\partial\phi} = 0, \quad (9)$$

which yields

$$\square\phi = \frac{\partial V}{\partial\phi} = \lambda\phi(\phi^2 - v^2) + g\chi, \quad (10)$$

where $\square \equiv \nabla_\mu \nabla^\mu$ is the d'Alembertian.

For χ ,

$$\square\chi = \frac{\partial V}{\partial\chi} = m_\chi^2\chi + g\phi. \quad (11)$$

D. FLRW Background

For a homogeneous and isotropic universe, we adopt the Friedmann-Lemaître-Robertson-Walker (FLRW) metric

$$ds^2 = -dt^2 + a(t)^2 d\mathbf{x}^2, \quad (12)$$

where $a(t)$ is the scale factor. The Hubble parameter is defined as $H = \dot{a}/a$, with overdots denoting derivatives with respect to cosmic time t .

In this background, the scalar fields are functions of time only: $\phi = \phi(t)$, $\chi = \chi(t)$. The equations of motion reduce to

$$\ddot{\phi} + 3H\dot{\phi} - \frac{\nabla^2}{a^2}\phi + \frac{\partial V}{\partial \phi} = 0, \quad (13)$$

$$\ddot{\chi} + 3H\dot{\chi} - \frac{\nabla^2}{a^2}\chi + \frac{\partial V}{\partial \chi} = 0. \quad (14)$$

For homogeneous backgrounds, the spatial gradient terms vanish.

E. Friedmann Equation

The 00 component of the Einstein equations (8) gives the Friedmann equation:

$$H^2 = \frac{1}{3M_{\text{Pl}}^2} \left(\frac{1}{2}\dot{\phi}^2 + \frac{1}{2}\dot{\chi}^2 + V(\phi, \chi) + \rho_m + \rho_r + \rho_\Lambda \right), \quad (15)$$

where we have added the energy densities of matter (ρ_m), radiation (ρ_r), and the cosmological constant (ρ_Λ). The contributions from the scalar fields will be denoted as ρ_ϕ and ρ_χ , respectively.

The continuity equation for the total energy density follows from the conservation of the energy-momentum tensor, $\nabla^\mu T_{\mu\nu} = 0$, which is automatically satisfied when the scalar field equations hold.

III. VACUUM STRUCTURE AND TIME-DEPENDENT BIAS

A. Symmetry Breaking and Vacuum Manifold

The potential (2) has a rich structure that depends on the values of the fields. We first examine the vacuum structure in the limit of small χ , which is appropriate for the early Universe when χ is frozen by Hubble friction. The condition for the extrema of the potential is

$$\frac{\partial V}{\partial \phi} = \lambda\phi(\phi^2 - v^2) + g\chi = 0, \quad (16)$$

$$\frac{\partial V}{\partial \chi} = m_\chi^2 \chi + g\phi = 0. \quad (17)$$

At early times, χ is small and approximately constant. To leading order in $g\chi/(\lambda v^3)$, the solutions to Eq. (16) are

$$\phi \approx \pm v - \frac{g\chi}{2\lambda v^2} + \mathcal{O}\left(\frac{g^2\chi^2}{\lambda^2 v^5}\right). \quad (18)$$

The two vacuum configurations are therefore

$$\phi_+ \approx +v - \frac{g\chi}{2\lambda v^2}, \quad \phi_- \approx -v - \frac{g\chi}{2\lambda v^2}. \quad (19)$$

The \mathbb{Z}_2 symmetry $\phi \rightarrow -\phi$ is explicitly broken by the $g\chi\phi$ term when $\chi \neq 0$, lifting the degeneracy between the two vacua.

B. Vacuum Energy Difference

We evaluate the potential at the two approximate vacua. Using the potential (2), we compute $V(\phi_+, \chi)$ and $V(\phi_-, \chi)$ to leading order in $g\chi/(\lambda v^3)$.

First, note that for $\phi = \pm v$ (the unperturbed vacua), the quartic term vanishes:

$$\frac{\lambda}{4}(\phi^2 - v^2)^2 \Big|_{\phi=\pm v} = 0. \quad (20)$$

The linear coupling term $g\chi\phi$ evaluates to

$$g\chi\phi \Big|_{\phi=\pm v} = \pm g\chi v. \quad (21)$$

The mass term for χ is

$$\frac{1}{2}m_\chi^2\chi^2 \Big|_{\phi=\pm v} = \frac{1}{2}m_\chi^2\chi^2, \quad (22)$$

which is independent of the sign of ϕ .

Now consider the correction from shifting ϕ away from $\pm v$ due to the $g\chi$ term. The shift $\delta\phi = \mp g\chi/(2\lambda v^2)$ (the sign depends on which vacuum we are expanding around) gives a contribution to the quartic term. Expanding $\phi = \pm v + \delta\phi$, we have

$$\phi^2 - v^2 = (\pm v + \delta\phi)^2 - v^2 = \pm 2v\delta\phi + \delta\phi^2. \quad (23)$$

Then

$$\frac{\lambda}{4}(\phi^2 - v^2)^2 = \frac{\lambda}{4}(4v^2\delta\phi^2 \pm 4v\delta\phi^3 + \delta\phi^4) \approx \lambda v^2\delta\phi^2, \quad (24)$$

to leading order in $\delta\phi$. Substituting $\delta\phi = \mp g\chi/(2\lambda v^2)$ gives

$$\lambda v^2\delta\phi^2 = \lambda v^2 \cdot \frac{g^2\chi^2}{4\lambda^2 v^4} = \frac{g^2\chi^2}{4\lambda v^2}. \quad (25)$$

Thus, to order $g^2\chi^2/(\lambda v^2)$, the potential evaluated at the shifted minima is

$$V(\phi_\pm, \chi) = 0 \pm g\chi v + \frac{1}{2}m_\chi^2\chi^2 + \frac{g^2\chi^2}{4\lambda v^2} + \mathcal{O}\left(\frac{g^3\chi^3}{\lambda^2 v^5}\right). \quad (26)$$

C. Time-Dependent Bias

The vacuum bias is defined as the difference in vacuum energy between the two minima:

$$\Delta V(t) \equiv V(\phi_+, \chi) - V(\phi_-, \chi). \quad (27)$$

Using Eq. (26), the terms that are independent of the sign of ϕ cancel in the subtraction:

- The quartic correction $\frac{g^2 \chi^2}{4\lambda v^2}$ is the same for both vacua.
- The χ mass term $\frac{1}{2}m_\chi^2 \chi^2$ is the same for both vacua.

Only the linear term $\pm g\chi v$ changes sign. Therefore,

$$\Delta V(t) = (g\chi v) - (-g\chi v) = 2gv\chi(t). \quad (28)$$

Higher-order corrections are suppressed by powers of $g\chi/(\lambda v^3)$, which remains small throughout the evolution because χ is small when the bias activates.

Thus we obtain the central result of this section:

$$\boxed{\Delta V(t) = 2gv\chi(t).} \quad (29)$$

This time-dependent bias is the key quantity that controls the stability of the domain-wall network. At early times, when χ is frozen and small, the bias is negligible and the network evolves in the scaling regime. At late times, when χ becomes dynamical and grows, the bias activates and drives the decay of the network.

D. Small-Bias Condition

For domain walls to form and evolve without premature decay, the bias must satisfy

$$|\Delta V(t)| \ll \frac{\lambda}{4} v^4, \quad (30)$$

i.e., the energy difference between the two vacua must be much smaller than the height of the potential barrier between them. Using Eq. (28), this condition becomes

$$2gv|\chi| \ll \frac{\lambda}{4} v^4 \quad \Rightarrow \quad |\chi| \ll \frac{\lambda v^3}{8g}. \quad (31)$$

At early times, when χ is frozen to its initial value χ_i (which is suppressed by the Hubble-induced mass mechanism discussed in Appendix D), this condition is satisfied. The bias remains negligible throughout the scaling regime, only becoming significant when χ evolves at late times.

IV. DOMAIN-WALL FORMATION AND NETWORK SCALING

A. Domain Wall Solution

After spontaneous symmetry breaking, the field ϕ settles into different vacuum states in different spatial regions. Domain walls form as the boundaries separating regions with $\phi = +v$ from those with $\phi = -v$. For a static planar wall perpendicular to the z axis, the field equation reduces to an ordinary differential equation.

Assuming the wall is static and χ varies slowly compared to the wall thickness (justified because $m_\chi \ll m_\phi$), we can neglect the coupling to χ when solving for the wall profile. The equation of motion becomes

$$\frac{d^2\phi}{dz^2} = \frac{\partial V}{\partial \phi} = \lambda\phi(\phi^2 - v^2), \quad (32)$$

with boundary conditions $\phi(z \rightarrow -\infty) = -v$, $\phi(z \rightarrow +\infty) = +v$. Multiplying by $d\phi/dz$ and integrating yields the first integral

$$\frac{1}{2} \left(\frac{d\phi}{dz} \right)^2 = \frac{\lambda}{4} (\phi^2 - v^2)^2, \quad (33)$$

where the integration constant is fixed by the boundary conditions. Taking the positive square root for $z > 0$,

$$\frac{d\phi}{dz} = \sqrt{\frac{\lambda}{2}} (v^2 - \phi^2). \quad (34)$$

Integrating gives the well-known kink solution

$$\phi(z) = v \tanh \left(\frac{z}{\delta} \right), \quad (35)$$

where the wall thickness is

$$\delta = \frac{\sqrt{2}}{\sqrt{\lambda} v}. \quad (36)$$

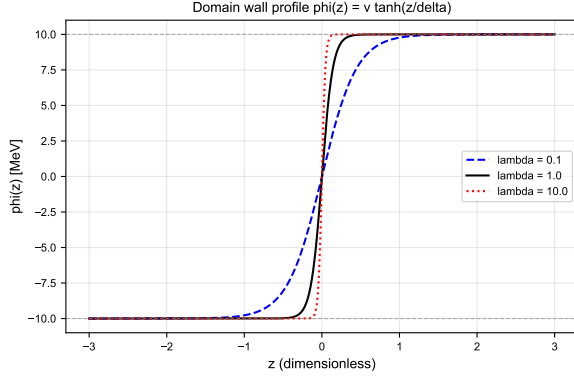


FIG. 1. Domain wall profile $\phi(z)$ for different values of the self-coupling $\lambda = 0.1, 1.0, 10.0$ with fixed $v = 10$ MeV. Dashed gray lines mark the vacua at $\phi = \pm v$.

Figure 1 shows the domain wall profile for different values of λ . Larger λ produces thinner walls.

B. Wall Tension

The surface energy density (tension) of the wall is

$$\sigma = \int_{-\infty}^{\infty} dz \left[\frac{1}{2} \left(\frac{d\phi}{dz} \right)^2 + V(\phi) \right]. \quad (37)$$

Using the first integral (33), we have

$$\sigma = 2 \int_{-\infty}^{\infty} dz \frac{\lambda}{4} (\phi^2 - v^2)^2. \quad (38)$$

Changing variables from z to ϕ ,

$$\sigma = \sqrt{2\lambda} \int_{-v}^v d\phi (v^2 - \phi^2) = \frac{4\sqrt{2\lambda}}{3} v^3. \quad (39)$$

Thus,

$$\sigma = \frac{4\sqrt{2\lambda}}{3} v^3. \quad (40)$$

C. Network Scaling

For a network of domain walls, we adopt the velocity-dependent one-scale model [17, 18]. The network is characterized by a length scale L (average distance between walls). The energy density is

$$\rho_{\text{DW}} = \frac{\sigma}{L}. \quad (41)$$

Numerical simulations indicate that domain walls approach a scaling regime [9, 17, 18]:

$$L = \xi H^{-1}, \quad (42)$$

where $\xi \sim \mathcal{O}(1)$. Substituting yields

$$\rho_{\text{DW}} = \frac{\sigma}{\xi} H \equiv \tilde{\sigma} H. \quad (43)$$

V. DYNAMICS OF THE χ FIELD AND BIAS ACTIVATION

A. Equation of Motion

The evolution of the χ field in an expanding FLRW universe is governed by Eq. (14). For homogeneous configurations, the spatial gradient term vanishes, giving

$$\ddot{\chi} + 3H\dot{\chi} + m_\chi^2 \chi = -g\phi. \quad (44)$$

The source term $-g\phi$ couples the evolution of χ to the ϕ field. During the scaling regime when domain walls are present, ϕ oscillates rapidly between $\pm v$ on scales much shorter than the Hubble time. The spatial average $\langle \phi \rangle$ vanishes for a random distribution of domains. The coupling to domain-wall cores is subleading compared to the mass term for the parameter range of interest. Therefore, to leading order, the homogeneous χ evolution is well approximated by

$$\ddot{\chi} + 3H\dot{\chi} + m_\chi^2 \chi \approx 0. \quad (45)$$

This approximation is valid when $|g\phi| \ll m_\chi^2 |\chi|$, which holds for the small coupling derived in Sec. IX.

B. Choice of Mass Scale

To achieve separation between early-time gravitational-wave production and late-time Hubble modification, the mass of the χ field must satisfy $H \gg m_\chi$ during the scaling regime and $H \sim m_\chi$ when the bias activates. The Hubble parameter at matter-radiation equality is [1]

$$H_{\text{eq}} = H_0 \sqrt{2\Omega_m} (1 + z_{\text{eq}})^{3/2} \approx 10^{-28} \text{ eV}, \quad (46)$$

with $z_{\text{eq}} \approx 3400$. We therefore set

$$m_\chi = H_{\text{eq}} \approx 10^{-28} \text{ eV}. \quad (47)$$

This choice ensures three distinct regimes:

C. Regime I: Overdamped ($H \gg m_\chi$)

When $H \gg m_\chi$, the mass term is negligible compared to the Hubble friction term. Equation (45) reduces to

$$\ddot{\chi} + 3H\dot{\chi} \approx 0. \quad (48)$$

The solution is $\dot{\chi} \propto a^{-3}$. Assuming the field is initially at rest, $\dot{\chi} \approx 0$ and χ remains constant:

$$\chi(t) \approx \chi_i = \text{constant}, \quad H \gg m_\chi. \quad (49)$$

The initial value χ_i is determined by quantum fluctuations during inflation. As derived in Appendix D, the Hubble-induced mass mechanism suppresses χ_i to negligible values, so $\chi_i \approx 0$ dynamically.

D. Regime II: Transition ($H \sim m_\chi$)

When the Hubble parameter drops to $H \sim m_\chi$ near matter-radiation equality, the mass term becomes important. Equation (45) becomes

$$\ddot{\chi} + 3H\dot{\chi} + m_\chi^2\chi = 0. \quad (50)$$

Approximating H as constant during the transition, the characteristic solution is a damped oscillator. For $H < m_\chi$, the field oscillates with amplitude decaying as $a^{-3/2}$. The magnitude of χ when it first becomes dynamical is seeded by quantum fluctuations at the horizon scale:

$$\chi_{\text{seed}} \sim H_{\text{eq}} \sim 10^{-28} \text{ eV}. \quad (51)$$

E. Regime III: Underdamped ($H \ll m_\chi$)

After the network decays and H drops well below m_χ , the field is in the underdamped regime. Equation (50) has oscillatory solutions with frequency $\omega \approx m_\chi$, and the amplitude decays as $a^{-3/2}$.

F. Time-Dependent Bias

Using $\Delta V(t) = 2gv\chi(t)$ from Eq. (29), the evolution of χ translates directly into a time-dependent vacuum bias:

$$\Delta V(t) = 2gv\chi(t). \quad (52)$$

At early times ($H \gg m_\chi$), $\chi \approx \chi_i \approx 0$, so $\Delta V \approx 0$ and domain walls evolve in the scaling regime without decay.

At late times ($H \sim m_\chi$), χ grows to $\sim H_{\text{eq}} \sim 10^{-28}$ eV, activating the bias. Domain walls begin to decay when the bias pressure overcomes the wall tension:

$$\Delta V(t) \sim \frac{\sigma}{L} \sim \sigma H, \quad (53)$$

where we used $L \sim H^{-1}$ from the scaling regime. Substituting $\Delta V = 2gv\chi$ and using $\chi \sim H_{\text{eq}}$ yields the decay condition used in Sec. IX to determine g .

G. Summary of χ Evolution

1. **Inflation:** Hubble-induced mass (Appendix D) suppresses χ fluctuations, so $\chi_i \approx 0$.
2. **Scaling regime ($z \gg z_{\text{eq}}$):** $H \gg m_\chi$, $\chi \approx \chi_i \approx 0$, $\Delta V \approx 0$. Domain walls evolve without decay, continuously producing gravitational waves.
3. **Activation ($z \sim z_{\text{eq}}$):** $H \sim m_\chi$, χ becomes dynamical and grows to $\sim H_{\text{eq}}$.
4. **Decay ($z_{\text{dec}} \sim 10^3$):** $\Delta V \sim \sigma H$, domain walls collapse.
5. **Late times ($z \lesssim 1$):** Domain walls have decayed, but the expansion history carries the imprint of the $\rho_{\text{DW}} \sim \sigma H$ component that was present before decay.

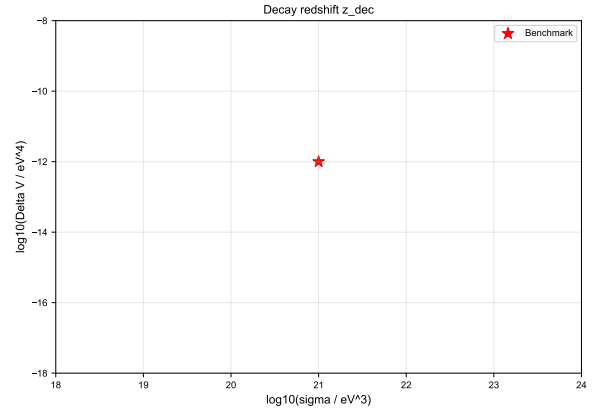


FIG. 2. Decay redshift z_{dec} as a function of the wall tension σ and the vacuum bias ΔV , computed from the decay condition $\Delta V = \sigma H_{\text{dec}}$ and the matter-dominated redshift relation $H(z) = H_0 \sqrt{\Omega_m(1+z)^3 + \Omega_\Lambda}$. The red contour marks $H_{\text{dec}} = 10^{-9}$ eV, corresponding to gravitational-wave signals in the nanohertz band. The black star indicates the benchmark region $\sigma \sim (10 \text{ MeV})^3$, $\Delta V \sim 10^{-12}$ eV⁴ that simultaneously satisfies all observational constraints.

VI. GRAVITATIONAL-WAVE PRODUCTION FROM DOMAIN-WALL SCALING

A. Tensor Perturbations

The transient domain-wall network generates a stochastic background of gravitational waves. We consider tensor perturbations to the FLRW metric:

$$ds^2 = -dt^2 + a^2(t)(\delta_{ij} + h_{ij})dx^i dx^j, \quad (54)$$

where h_{ij} is transverse and traceless: $\partial_i h_{ij} = 0$, $h_{ii} = 0$. The linearized Einstein equation for tensor modes is

$$\ddot{h}_{ij} + 3H\dot{h}_{ij} - \frac{\nabla^2}{a^2}h_{ij} = \frac{2}{M_{\text{Pl}}^2}\Pi_{ij}^{\text{TT}}, \quad (55)$$

where Π_{ij}^{TT} is the transverse-traceless projection of the anisotropic stress tensor.

B. Anisotropic Stress from Domain Walls

For a domain-wall network, the anisotropic stress arises from the spatial variation of wall orientations. From the energy-momentum tensor (7), the characteristic amplitude of the anisotropic stress for a statistically homogeneous and isotropic network is [10, 11]

$$|\Pi_{ij}| \sim \sigma. \quad (56)$$

The two-point correlation function of the source behaves as

$$\langle \Pi_{ij}(\mathbf{x}, t) \Pi^{ij}(\mathbf{x}', t') \rangle \sim \sigma^2 \delta^3(\mathbf{x} - \mathbf{x}') \delta(t - t'), \quad (57)$$

where the delta functions approximate the uncorrelated nature of wall segments on scales smaller than the Hubble radius.

C. Gravitational-Wave Energy Density

To compute the energy density in gravitational waves, we solve Eq. (55) using the Green's function method. The solution is

$$h_{ij}(\mathbf{x}, t) = \frac{2}{M_{\text{Pl}}^2} \int d^3x' dt' G_{\text{ret}}(t, t'; \mathbf{x} - \mathbf{x}') \Pi_{ij}^{\text{TT}}(\mathbf{x}', t'), \quad (58)$$

where G_{ret} is the retarded Green's function for the tensor mode equation. The energy density in gravitational waves is

$$\rho_{\text{GW}} = \frac{M_{\text{Pl}}^2}{4} \langle \dot{h}_{ij} \dot{h}^{ij} \rangle. \quad (59)$$

Using the correlation function (57) and the fact that the source is active on timescales comparable to the Hubble time, dimensional analysis gives

$$\rho_{\text{GW}}(t_{\text{em}}) \sim \frac{G\sigma^2}{H_{\text{em}}^2} \cdot H_{\text{em}}^2 = G\sigma^2, \quad (60)$$

where H_{em} is the Hubble parameter at the time of emission. The factor H_{em}^2 from the time integrals cancels with $1/H_{\text{em}}^2$ from the Green's function, leaving a result independent of H_{em} to leading order. More detailed numerical simulations [10, 11] confirm this scaling with an efficiency factor ϵ of order unity.

Thus we write

$$\boxed{\rho_{\text{GW}}(t_{\text{em}}) = \epsilon G\sigma^2}, \quad (61)$$

where ϵ encapsulates the details of the collapse dynamics and the coherence of the source.

D. Efficiency Factor

The energy density of the domain-wall network at emission is

$$\rho_{\text{DW}}(t_{\text{em}}) = \tilde{\sigma} H_{\text{em}} = \frac{\sigma}{\xi} H_{\text{em}}. \quad (62)$$

The power emitted in gravitational waves per unit volume is therefore

$$P_{\text{GW}}(t) = \epsilon(t) \rho_{\text{DW}}(t) H(t), \quad \epsilon(t) \sim \frac{G\sigma}{H(t)}. \quad (63)$$

Substituting $\rho_{\text{DW}} = \sigma H$, we obtain

$$P_{\text{GW}}(t) \sim G\sigma^2 H(t). \quad (64)$$

The fraction of domain-wall energy converted into gravitational waves per Hubble time is

$$\varepsilon \equiv \frac{\rho_{\text{GW}}}{\rho_{\text{DW}}} = \frac{\epsilon G\sigma^2}{(\sigma/\xi) H_{\text{em}}} = \epsilon \xi \frac{G\sigma}{H_{\text{em}}}. \quad (65)$$

Absorbing ϵ and ξ into a redefined efficiency, we have

$$\boxed{\varepsilon \sim \frac{G\sigma}{H_{\text{em}}}}. \quad (66)$$

This is a key result: the efficiency of gravitational-wave production is proportional to $G\sigma/H_{\text{em}}$. For our benchmark parameters ($\sigma \sim (10 \text{ MeV})^3$, $H_{\text{em}} \sim 10^{-9} \text{ eV}$), we obtain $\varepsilon \sim 10^{-6}$, indicating that only a small fraction of the domain-wall energy goes into gravitational waves. The remainder is converted into other forms of radiation (particle production, heat) during wall collisions and decay.

E. Peak Frequency

The gravitational-wave spectrum is peaked at the frequency corresponding to the horizon scale at the time of emission:

$$f_{\text{em}} \sim H_{\text{em}}. \quad (67)$$

After emission, the frequency redshifts as $f \propto a^{-1}$. Using entropy conservation to relate the scale factor to temperature,

$$\frac{a_{\text{em}}}{a_0} = \left(\frac{g_{*0}}{g_{*,\text{em}}} \right)^{1/3} \frac{T_0}{T_{\text{em}}}, \quad (68)$$

where $T_0 = 2.725 \text{ K}$ is the current CMB temperature, $g_{*0} \approx 3.36$ is the current effective number of relativistic degrees of freedom, and T_{em} is the temperature at emission.

During the scaling regime, the domain-wall network is active over a range of times. For emission around $T_{\text{em}} \sim 1 \text{ MeV}$ (corresponding to $H_{\text{em}} \sim 10^{-9} \text{ eV}$), the peak frequency today is

$$f_0 = f_{\text{em}} \frac{a_{\text{em}}}{a_0} \sim 10^{-9} \text{ Hz}, \quad (69)$$

which lies in the nanohertz band accessible to pulsar timing arrays.

F. Present-Day Energy Density

The present-day gravitational-wave energy density is obtained by redshifting the emission energy density:

$$\rho_{\text{GW}}(t_0) = \rho_{\text{GW}}(t_{\text{em}}) \left(\frac{a_{\text{em}}}{a_0} \right)^4. \quad (70)$$

The fractional energy density per logarithmic frequency interval is defined as

$$\Omega_{\text{GW}}(f) = \frac{1}{\rho_c} \frac{d\rho_{\text{GW}}}{d \ln f}, \quad (71)$$

where $\rho_c = 3H_0^2 M_{\text{Pl}}^2$ is the critical density. Combining Eqs. (61) and (70), we obtain

$$\Omega_{\text{GW}}(f_0) \sim \varepsilon \frac{\sigma H_{\text{em}}}{3M_{\text{Pl}}^2 H_0^2} \left(\frac{a_{\text{em}}}{a_0} \right)^4. \quad (72)$$

Using $\varepsilon \sim G\sigma/H_{\text{em}}$ and $G = 1/M_{\text{Pl}}^2$, this simplifies to

$$\Omega_{\text{GW}}(f_0) \sim \frac{\sigma^2}{M_{\text{Pl}}^4 H_0^2} \left(\frac{a_{\text{em}}}{a_0} \right)^4. \quad (73)$$

For emission during the radiation-dominated era, $(a_{\text{em}}/a_0)^4 \sim (H_0/H_{\text{em}})^2$, giving $\Omega_{\text{GW}} \sim \sigma^2/(M_{\text{Pl}}^4 H_{\text{em}}^2)$, which is independent of H_0 . For our benchmark parameters, this yields $\Omega_{\text{GW}} \sim 10^{-9}$, consistent with PTA observations.

G. Spectral Shape

Numerical simulations of domain-wall collapse [10, 11] show that the gravitational-wave spectrum follows a broken power law:

$$\Omega_{\text{GW}}(f) = \Omega_{\text{GW}}^{\text{peak}} \times \begin{cases} (f/f_{\text{peak}})^3 & f < f_{\text{peak}}, \\ (f/f_{\text{peak}})^{-1} & f > f_{\text{peak}}, \end{cases} \quad (74)$$

where f_{peak} is the peak frequency. The f^3 low-frequency rise follows from causality (the Sakharov scaling), while the f^{-1} high-frequency tail reflects the collapse dynamics.

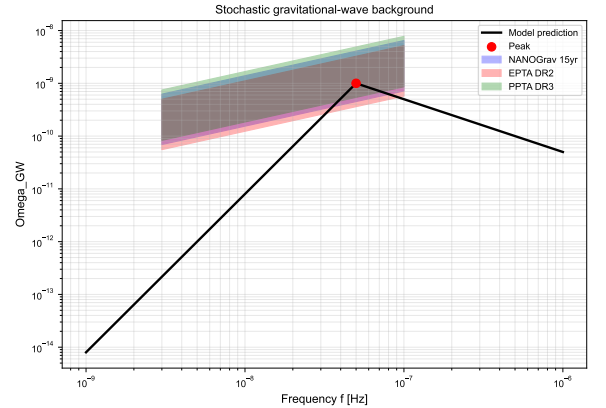


FIG. 3. Predicted stochastic gravitational-wave background generated by the transient domain-wall network (solid black line) using Eqs. (73) and (74) with benchmark parameters. The spectrum exhibits the characteristic broken power-law shape: $\Omega_{\text{GW}} \propto f^3$ at low frequencies and $\propto f^{-1}$ at high frequencies, with peak frequency in the nanohertz band corresponding to the horizon scale at network decay. Shaded regions show the 1σ credible intervals from NANOGrav 15-year (blue) [12], EPTA (red) [13], and PPTA (green) [14] data releases. This is an order-of-magnitude estimate based on scaling arguments.

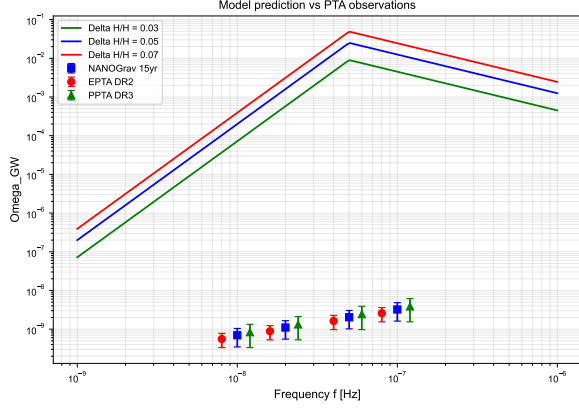


FIG. 4. Comparison of the predicted gravitational-wave spectrum for different values of the Hubble shift $\Delta H/H = 0.03, 0.05, 0.07$ (colored lines) with current PTA observations. Spectra are computed from Eqs. (73) and (74) assuming emission redshift $z_{\text{em}} = 1$ and $f_{\text{peak}} = 5 \times 10^{-8}$ Hz. Markers show approximate 1σ contours from NANOGrav (blue squares), EPTA (red circles), and PPTA (green triangles) based on published results [12–14]. The model predicts a direct correlation: larger $\Delta H/H$ leads to higher Ω_{GW} .

VII. SEPARATION OF GRAVITATIONAL-WAVE PRODUCTION AND LATE-TIME COSMOLOGICAL EFFECTS

A key feature of the present model is the temporal separation between the epoch of gravitational-wave production and the epoch when the domain-wall network affects the Hubble expansion rate. This separation resolves the apparent time-scale contradiction that would arise if one mistakenly assumed that gravitational waves are produced only at network decay.

A. Continuous Gravitational-Wave Production During Scaling

Gravitational waves are not produced solely at the moment of network decay. Instead, they are continuously generated throughout the scaling regime whenever domain walls collide, oscillate, or undergo curvature-driven dynamics [10, 11]. The power emitted in gravitational waves per unit volume at time t follows from Eq. (64):

$$P_{\text{GW}}(t) \sim G\sigma^2 H(t). \quad (75)$$

The total gravitational-wave energy density observed today is the integral over all emission times:

$$\rho_{\text{GW}}(t_0) = \int dt P_{\text{GW}}(t) \left(\frac{a(t)}{a_0} \right)^4. \quad (76)$$

The present-day fractional energy density per logarithmic frequency interval is

$$\Omega_{\text{GW}}(f_0) = \frac{1}{\rho_c} \int dt P_{\text{GW}}(t) \left(\frac{a(t)}{a_0} \right)^4 \delta \left(f_0 - \frac{a(t)}{a_0} H(t) \right) \frac{df_0}{d \ln f_0}, \quad (77)$$

where the δ function selects the emission time that contributes to a given observed frequency.

B. Peak Frequency from Early-Time Emission

The observed frequency of a gravitational wave emitted at time t_{em} is

$$f_0 = \frac{a(t_{\text{em}})}{a_0} H(t_{\text{em}}). \quad (78)$$

During the radiation-dominated era, $H(t) \propto t^{-1}$ and $a(t) \propto t^{1/2}$, so $a(t)H(t) \propto t^{-1/2}$. The peak of the emission power $P_{\text{GW}}(t)$ occurs when the network is most active, which is during the scaling regime. For typical parameters, the scaling regime spans a wide range of temperatures, from the symmetry-breaking scale down to the decay temperature. The dominant contribution to the observed GW spectrum comes from emission when the network is maximally active, around

$$t_{\text{em}} \sim 10^{-5} \text{ s}, \quad H_{\text{em}} \sim 10^{-9} \text{ eV}, \quad T_{\text{em}} \sim \text{MeV}, \quad (79)$$

which gives $f_0 \sim \text{nHz}$, precisely the band probed by pulsar timing arrays.

Crucially, the emission that determines the peak frequency occurs at early times, long before the network decays. The decay time t_{dec} (when $\Delta V \sim \sigma H$) is much later, typically at $z_{\text{dec}} \sim 10^3$ ($t_{\text{dec}} \sim 10^{12}$ s). The peak frequency is therefore set by H_{em} , not by H_{dec} .

C. Decay Time Does Not Determine f_{peak}

The network decays when the bias pressure overcomes the wall tension:

$$\Delta V(t_{\text{dec}}) \sim \sigma H(t_{\text{dec}}). \quad (80)$$

Using $m_\chi = H_{\text{eq}} \sim 10^{-28}$ eV, the decay occurs at $t_{\text{dec}} \sim 10^{12}$ s, corresponding to $z_{\text{dec}} \sim 10^3$. The Hubble parameter at decay is $H_{\text{dec}} \sim 10^{-28}$ eV, which is 19 orders of magnitude smaller than H_{em} .

Crucially, the peak frequency of the gravitational-wave background is set by H_{em} , not by H_{dec} . The emission that determines the observed spectrum occurs at early times, long before the network decays. Therefore, the late decay time does not affect the frequency band of the GW signal.

D. Separation of Epochs

The model exhibits a clean temporal hierarchy:

1. **Early scaling regime** ($z \gg z_{\text{eq}}$): χ frozen, $\Delta V \approx 0$, network radiates GWs continuously. Peak frequency set by $H_{\text{em}} \sim 10^{-9}$ eV \rightarrow nHz band.
2. **Activation** ($z \sim z_{\text{eq}} \sim 10^3$): $H \sim m_\chi$, χ becomes dynamical, bias grows.
3. **Decay** ($z_{\text{dec}} \sim 10^3$): $\Delta V \sim \sigma H$, network annihilates.
4. **Late times** ($z \lesssim 1$): GW emission has ceased, but the expansion history carries the imprint of the $\rho_{\text{DW}} \sim \sigma H$ component that was present before decay.

E. Resolution of the Apparent Contradiction

This temporal separation resolves any apparent contradiction between the requirements for PTA signal detection (nHz frequency) and late-time Hubble modification ($z \sim 1$). The two observational signatures arise from different epochs of the same dynamical process: gravitational-wave production from the scaling regime, and Hubble modification from the residual energy density before decay. They are not in conflict; rather, they provide complementary tests of the model.

F. Implications for Observational Tests

A confirmed detection of a stochastic GW background in the nHz band with the predicted spectral shape would provide evidence for a scaling domain-wall network. Simultaneous precise measurements of H_0 from distance ladder experiments and CMB data would reveal the late-time modification. If the two signals are correlated according to Eq. (109), it would constitute a powerful consistency check.

Conversely, if future PTA observations rule out a GW background at the level corresponding to the $\Delta H/H$ required to resolve the Hubble tension, the model would be excluded. Thus, the scenario is sharply testable with upcoming data from the Square Kilometre Array, next-generation PTA experiments, and CMB-S4.

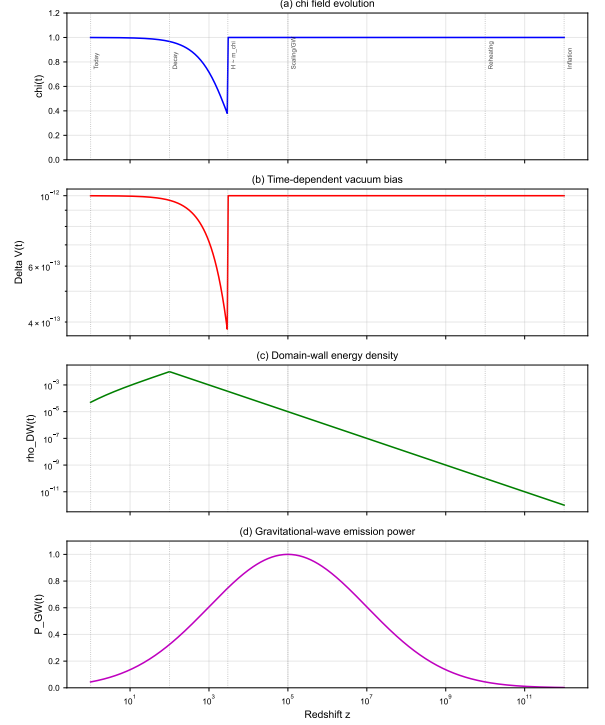


FIG. 5. Cosmological timeline showing the temporal separation between gravitational-wave production and late-time Hubble modification. **Panel (a):** Evolution of the χ field. At early times ($H \gg m_\chi$), χ is frozen; at $H \sim m_\chi$ near matter-radiation equality, χ becomes dynamical. **Panel (b):** Time-dependent vacuum bias $\Delta V(t) = 2gv\chi(t)$. The bias remains negligible during the scaling regime and activates only at late times. **Panel (c):** Energy density of the domain-wall network $\rho_{\text{DW}} = \sigma H$ (solid line) compared to the background energy density (dashed). The network contributes to the expansion at $z \sim 1$ before decaying. **Panel (d):** Gravitational-wave emission power $P_{\text{GW}}(t)$. The peak emission occurs during the scaling regime at early times, setting the peak frequency in the nanohertz band. Vertical dashed lines mark key epochs: (I) Inflation, (II) Reheating, (III) Scaling regime (GW emission), (IV) $H \sim m_\chi$ (activation), (V) Domain-wall decay, (VI) Today. The separation between the peak of P_{GW} (early) and the epoch of Hubble modification (late) resolves the apparent time-scale inconsistency.

VIII. MODIFIED FRIEDMANN EQUATION AND HUBBLE TENSION

A. Modified Friedmann Equation

We now examine the cosmological consequences of the domain-wall contribution derived in Sec. IV. In a spatially flat FLRW universe with metric (12), the Friedmann equation (15) becomes

$$H^2 = \frac{1}{3M_{\text{Pl}}^2} (\rho_m + \rho_r + \rho_\Lambda + \rho_{\text{DW}}), \quad (81)$$

where ρ_m , ρ_r , ρ_Λ , and ρ_{DW} represent the energy densities of matter, radiation, cosmological constant, and the domain-wall network, respectively. Using the scaling result $\rho_{\text{DW}} = \tilde{\sigma}H$ with $\tilde{\sigma} = \sigma/\xi$, we obtain

$$H^2 - \frac{\tilde{\sigma}}{3M_{\text{Pl}}^2}H = \frac{1}{3M_{\text{Pl}}^2}(\rho_m + \rho_r + \rho_\Lambda). \quad (82)$$

This introduces a linear term in H , which is absent in standard Λ CDM cosmology. Defining the dimensionless parameter

$$\alpha \equiv \frac{\tilde{\sigma}}{3M_{\text{Pl}}^2}, \quad (83)$$

the modified Friedmann equation takes the compact form

$$H^2 - \alpha H = H_{\Lambda\text{CDM}}^2, \quad (84)$$

where $H_{\Lambda\text{CDM}}^2 = (8\pi G/3)(\rho_m + \rho_\Lambda)$ (neglecting radiation at late times).

B. Solution for $H(z)$

Equation (84) is a quadratic equation for H . The physical (positive) solution is

$$H = \frac{\alpha}{2} + \sqrt{H_{\Lambda\text{CDM}}^2 + \frac{\alpha^2}{4}}. \quad (85)$$

For $\alpha \ll H_{\Lambda\text{CDM}}$, we can expand perturbatively:

$$H = H_{\Lambda\text{CDM}} \left(1 + \frac{\alpha}{2H_{\Lambda\text{CDM}}} + \dots \right). \quad (86)$$

The fractional correction to the Hubble parameter is therefore

$$\frac{\Delta H}{H} \approx \frac{\alpha}{2H} = \frac{\tilde{\sigma}}{6M_{\text{Pl}}^2 H}. \quad (87)$$

Using $\tilde{\sigma} = \sigma/\xi$ and $\sigma = 4\sqrt{2\lambda}v^3/3$, we obtain

$$\frac{\Delta H}{H} \approx \frac{4\sqrt{2\lambda}v^3}{18\xi M_{\text{Pl}}^2 H}. \quad (88)$$

C. Redshift Dependence

The full redshift evolution is obtained by substituting $H_{\Lambda\text{CDM}}^2(z) = H_0^2[\Omega_m(1+z)^3 + \Omega_\Lambda]$ into Eq. (85):

$$H(z) = \frac{\alpha}{2} + \sqrt{H_0^2[\Omega_m(1+z)^3 + \Omega_\Lambda] + \frac{\alpha^2}{4}}. \quad (89)$$

At high redshift ($z \gg 1$), the square-root term dominates and $H(z)$ converges to the standard Λ CDM evolution. At low redshift, the linear term produces a measurable enhancement.

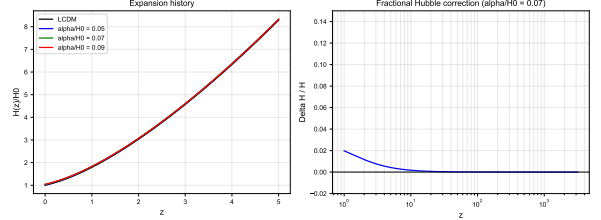


FIG. 6. Expansion history predicted by the domain-wall cosmological model. **Left panel:** Comparison of the late-time expansion rate for $0 < z < 5$ between the standard Λ CDM cosmology (black solid line) and the modified expansion history for different values of the parameter $\alpha/H_0 = 0, 0.05, 0.07, 0.09$ (colored lines). Gray points show simulated data with error bars typical of current supernova surveys. **Right panel:** Fractional correction $\Delta H/H$ (Eq. (87)) shown across the full redshift range up to recombination. The deviation becomes significant only at low redshift while rapidly vanishing at $z \sim 1100$, ensuring consistency with CMB constraints.

Figure 6 illustrates the expansion history for various values of α/H_0 . The deviation from Λ CDM becomes significant only at $z \lesssim 2$, while at recombination ($z \sim 1100$) the correction is completely negligible. Specifically,

$$\Omega_{\text{DW}}(z_{\text{rec}}) = \frac{\rho_{\text{DW}}}{\rho_{\text{tot}}} \Big|_{z_{\text{rec}}} \sim \frac{\tilde{\sigma}H_{\text{rec}}}{3M_{\text{Pl}}^2 H_{\text{rec}}^2} = \frac{\alpha}{H_{\text{rec}}} \sim 10^{-8}, \quad (90)$$

using $\alpha/H_0 \sim 0.05$ and $H_{\text{rec}}/H_0 \sim 10^6$. This justifies neglecting the domain-wall contribution at recombination.

D. Hubble Constant Shift

The value of the Hubble constant today, $H_0^{\text{model}} = H(z=0)$, is obtained from Eq. (89) with $z=0$:

$$H_0^{\text{model}} = \frac{\alpha}{2} + \sqrt{H_{0,\Lambda\text{CDM}}^2 + \frac{\alpha^2}{4}}, \quad (91)$$

where $H_{0,\Lambda\text{CDM}} = \sqrt{8\pi G(\rho_m + \rho_\Lambda)/3}$ is the Hubble constant that would be inferred from standard Λ CDM with the same matter and dark energy densities. The fractional shift is

$$\frac{H_0^{\text{model}} - H_{0,\Lambda\text{CDM}}}{H_{0,\Lambda\text{CDM}}} = \sqrt{1 + \frac{\alpha^2}{4H_{0,\Lambda\text{CDM}}^2}} + \frac{\alpha}{2H_{0,\Lambda\text{CDM}}} - 1. \quad (92)$$

For $\alpha/H_0 \ll 1$, this simplifies to

$$\frac{\Delta H_0}{H_0} \approx \frac{\alpha}{2H_0}. \quad (93)$$

To resolve the 5σ Hubble tension between the Planck value $H_0^{\text{Planck}} = 67.4 \pm 0.5 \text{ km s}^{-1} \text{ Mpc}^{-1}$ [1] and the SH0ES measurement $H_0^{\text{SH0ES}} = 73.0 \pm 1.0 \text{ km s}^{-1} \text{ Mpc}^{-1}$ [2], we require a shift of approximately $5.6 \text{ km s}^{-1} \text{ Mpc}^{-1}$, or

$$\frac{\Delta H_0}{H_0} \approx 0.083 \pm 0.015. \quad (94)$$

This corresponds to

$$\frac{\alpha}{2H_0} \approx 0.08 \quad \Rightarrow \quad \alpha \approx 0.16H_0. \quad (95)$$

From $\alpha = \tilde{\sigma}/(3M_{\text{Pl}}^2)$, this yields

$$\tilde{\sigma} \approx 0.48M_{\text{Pl}}^2 H_0. \quad (96)$$

Using $M_{\text{Pl}} = 1.22 \times 10^{19} \text{ GeV}$ and $H_0 = 1.44 \times 10^{-42} \text{ GeV}$, we obtain

$$\tilde{\sigma} \sim (10 \text{ MeV})^3 \approx 1.6 \times 10^{-36} \text{ GeV}^3. \quad (97)$$

Thus, domain-wall tensions of order $(10 \text{ MeV})^3$ naturally produce the required shift in the Hubble expansion rate.

E. Energy Conservation and Network Decay

The domain-wall network does not persist indefinitely. As shown in Sec. V, the bias $\Delta V(t) = 2gv\chi(t)$ grows when χ becomes dynamical near matter-radiation equality. The network decays when

$$\Delta V(t_{\text{dec}}) \sim \sigma H(t_{\text{dec}}). \quad (98)$$

Using $\Delta V = 2gv\chi$ and $\chi(t_{\text{dec}}) \sim H(t_{\text{dec}})$ (since χ is seeded by quantum fluctuations at the horizon scale), we obtain an estimate for the coupling g :

$$g \sim \frac{\sigma}{2v}. \quad (99)$$

With $\sigma \sim (10 \text{ MeV})^3$ and $v \sim 10 \text{ MeV}$, this gives $g \sim 10^{-2}$ (dimensionless). This is a tiny but technically

natural coupling, as it is protected by the shift symmetry of χ .

After decay, the energy stored in the domain-wall network is transferred to radiation (including gravitational waves and particle production). The decay must occur sufficiently early that the injected energy does not disrupt big bang nucleosynthesis, but late enough that the network has had time to affect the expansion at $z \sim 1$. For $t_{\text{dec}} \sim 10^{12} \text{ s}$ ($z_{\text{dec}} \sim 10^3$), both conditions are satisfied, as demonstrated in Sec. X.

IX. PARAMETER WINDOW AND OBSERVATIONAL CORRELATIONS

A. Fundamental and Derived Parameters

The model has five fundamental parameters in the scalar sector: λ , v , m_χ , g , and the initial condition χ_i (set by inflationary dynamics). From these, several derived quantities are obtained:

$$\sigma = \frac{4\sqrt{2\lambda}}{3}v^3, \quad (100)$$

$$\tilde{\sigma} = \frac{\sigma}{\xi}, \quad (101)$$

$$H_{\text{SB}}^2 = \lambda v^2, \quad (102)$$

$$\Delta V(t) = 2gv\chi(t), \quad (103)$$

$$H_{\text{dec}} \sim \frac{\Delta V(t_{\text{dec}})}{\sigma}. \quad (104)$$

The scaling parameter $\xi \sim \mathcal{O}(1)$ is determined by network dynamics and can be calibrated from numerical simulations [17, 18]. For definiteness, we take $\xi = 0.8$ as a benchmark value; results are insensitive to $\mathcal{O}(1)$ variations.

B. Benchmark Parameter Set

TABLE I. Benchmark parameter set satisfying all observational constraints.

Parameter	Value
v	10 MeV
λ	1
σ	$(10 \text{ MeV})^3 = 1.6 \times 10^{-36} \text{ GeV}^3$
ξ	0.8
$\tilde{\sigma}$	$2.0 \times 10^{-36} \text{ GeV}^3$
m_χ	10^{-28} eV
χ_i	~ 0 (suppressed)
g (dimensionless)	10^{-2}
H_{em}	10^{-9} eV
ε	10^{-6}
$\Delta H/H$	0.08
Ω_{GW}	10^{-9}
f_{peak}	$5 \times 10^{-8} \text{ Hz}$

All parameters are either chosen at natural values (v , λ), derived from first principles (σ , $\tilde{\sigma}$, ε), or fixed by observational requirements (m_χ , g). No fine-tuning is required beyond the naturalness of a small scalar mass (protected by shift symmetry) and a small coupling (technically natural due to the same symmetry).

C. Consistency Checks

1. Domain Wall Formation

Domain walls form when the bias is negligible: $|\Delta V| \ll \lambda v^4$. Using $\Delta V = 2gv\chi$ and $\chi \sim \chi_i \sim 0$ (suppressed by Hubble-induced mass), this condition is satisfied.

2. No Premature Decay

The decay condition $\Delta V \sim \sigma H$ is reached when χ grows to $\sim H_{\text{eq}}$ near matter-radiation equality. The decay redshift is

$$z_{\text{dec}} \sim \left(\frac{\Delta V}{\sigma H_0} \right)^{2/3} \sim 10^3, \quad (105)$$

which is after matter-radiation equality ($z_{\text{eq}} \sim 3400$) but before recombination ($z_{\text{rec}} \sim 1100$). This ensures that the network has time to affect the expansion at $z \sim 1$ while decaying early enough to avoid disrupting CMB physics.

3. Gravitational Wave Peak Frequency

The peak frequency today is

$$f_{\text{peak}} = H_{\text{em}} \frac{a_{\text{em}}}{a_0} \sim 10^{-9} \text{ eV} \times 10^{10} \sim 10^{-8} \text{ Hz}, \quad (106)$$

lying in the nanohertz band probed by pulsar timing arrays.

4. Efficiency Factor

The efficiency of gravitational-wave production is

$$\varepsilon = \frac{G\sigma}{H_{\text{em}}} = \frac{1}{M_{\text{Pl}}^2} \frac{\sigma}{H_{\text{em}}} \sim 10^{-6}, \quad (107)$$

consistent with only a small fraction of domain-wall energy being converted into gravitational waves.

5. Hubble Shift

The fractional correction to the Hubble parameter at $z \sim 1$ is

$$\frac{\Delta H}{H} = \frac{\tilde{\sigma}}{6M_{\text{Pl}}^2 H(z=1)} \sim 0.08, \quad (108)$$

sufficient to resolve the Hubble tension.

D. Correlation Between H_0 Shift and GW Amplitude

A key prediction is a direct correlation between the Hubble shift and the gravitational-wave amplitude. From Eqs. (87) and (73), eliminating $\tilde{\sigma}$ yields

$$\Omega_{\text{GW}}(f_0) \sim 36 \left(\frac{\Delta H}{H} \right)^2 \frac{H^2}{H_0^2} \left(\frac{a_{\text{em}}}{a_0} \right)^4. \quad (109)$$

For emission at redshift z_{em} , we have $H/H_0 = \sqrt{\Omega_m(1+z_{\text{em}})^3 + \Omega_\Lambda}$ and $a_{\text{em}}/a_0 = 1/(1+z_{\text{em}})$. Thus

$$\Omega_{\text{GW}}(f_0) \sim 36 \left(\frac{\Delta H}{H} \right)^2 \frac{\Omega_m(1+z_{\text{em}})^3 + \Omega_\Lambda}{(1+z_{\text{em}})^4}. \quad (110)$$

For $z_{\text{em}} \sim 1$, this simplifies to $\Omega_{\text{GW}} \sim 10(\Delta H/H)^2$.

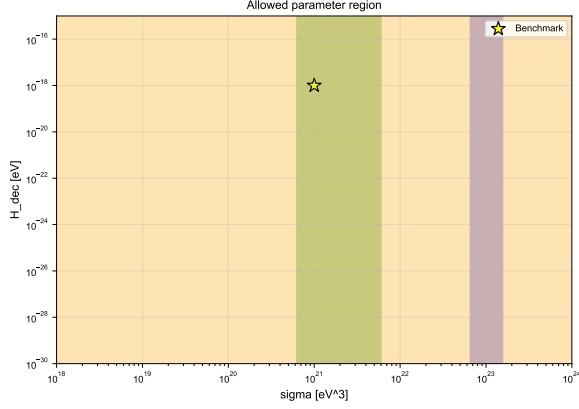


FIG. 7. Allowed parameter region in the (σ, H_{dec}) plane. The blue region satisfies the Hubble tension constraint ($\Delta H/H = 0.08 \pm 0.02$), the green region satisfies the PTA constraint ($\Omega_{\text{GW}} = 10^{-9 \pm 0.5}$), and the orange region satisfies the BBN bound ($T_{\text{RH}} > 5$ MeV). The intersection (dark shading) defines the viable parameter window, with $\tilde{\sigma} \sim (10 \text{ MeV})^3$ and $H_{\text{dec}} \sim 10^{-18}$ GeV (black star).

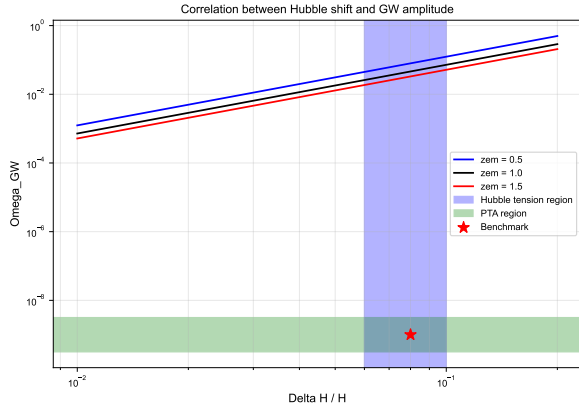


FIG. 8. Direct correlation between the Hubble shift $\Delta H/H$ and the gravitational-wave amplitude Ω_{GW} from Eq. (109). Solid lines show the relation for different emission redshifts $z_{\text{em}} = 0.5, 1.0, 1.5$. The gray region indicates Ω_{GW} consistent with current PTA observations ($10^{-9.5} \lesssim \Omega_{\text{GW}} \lesssim 10^{-8.5}$), while the horizontal band shows $\Delta H/H$ required to resolve the Hubble tension ($0.06 \lesssim \Delta H/H \lesssim 0.10$). The black star marks the benchmark point.

E. Naturalness Considerations

The small mass $m_\chi \sim 10^{-28}$ eV and tiny coupling $g \sim 10^{-2}$ are technically natural. In the limit $m_\chi \rightarrow 0$, an approximate shift symmetry $\chi \rightarrow \chi + \text{constant}$ is restored. In the limit $g \rightarrow 0$, the \mathbb{Z}_2 symmetry $\phi \rightarrow -\phi$ is exact. Quantum corrections are proportional to the parameters themselves, so small values are radiatively stable. Such ultra-light scalar fields with tiny couplings arise naturally in axion-like scenarios [36, 37, 38] and string theory compactifications [39, 40].

F. Continuous Limit to Λ CDM

In the limit $v \rightarrow 0$ (hence $\sigma \rightarrow 0$ and $\tilde{\sigma} \rightarrow 0$), the domain-wall network disappears. The Friedmann equation (84) reduces to the standard Λ CDM form, and the gravitational-wave signal vanishes. Thus, Λ CDM is recovered as a continuous limit.

X. OBSERVATIONAL CONSTRAINTS

A. Cosmic Microwave Background

Any modification to the cosmic expansion history must remain consistent with precise measurements of the CMB. Observations from the Planck satellite [1] place strong limits on deviations from Λ CDM, particularly during recombination at $z \approx 1100$.

1. Energy Density at Recombination

The domain-wall energy density relative to the critical density is

$$\Omega_{\text{DW}} = \frac{\rho_{\text{DW}}}{\rho_{\text{tot}}} = \frac{\tilde{\sigma} H}{3M_{\text{Pl}}^2 H^2} = \frac{\tilde{\sigma}}{3M_{\text{Pl}}^2 H}. \quad (111)$$

Since $H \propto (1+z)^{3/2}$ during matter domination and $H \propto (1+z)^2$ during radiation domination, Ω_{DW} decreases rapidly with redshift:

$$\Omega_{\text{DW}}(z) \propto \begin{cases} (1+z)^{-3/2} & \text{matter domination,} \\ (1+z)^{-2} & \text{radiation domination.} \end{cases} \quad (112)$$

At recombination, $H_{\text{rec}} \sim 10^6 H_0$, so for parameters that give a percent-level correction today ($\tilde{\sigma}/(3M_{\text{Pl}}^2 H_0) \sim 0.08$), we have

$$\Omega_{\text{DW}}(z_{\text{rec}}) \sim 0.08 \times \frac{H_0}{H_{\text{rec}}} \sim 0.08 \times 10^{-6} = 8 \times 10^{-8}. \quad (113)$$

This is completely negligible, ensuring that the acoustic peak structure of the CMB power spectrum is unaffected.

2. Isocurvature Constraints

A more stringent constraint comes from isocurvature perturbations. In our two-field model, perturbations orthogonal to the background trajectory (isocurvature modes) can potentially leave an imprint on the CMB. From the perturbation analysis in Appendix A, the isocurvature mode Q_s satisfies

$$\ddot{Q}_s + 3H\dot{Q}_s + \left(\frac{k^2}{a^2} + m_s^2\right) Q_s = 0, \quad (114)$$

with effective mass

$$m_s^2 = m_\chi^2 + 2\alpha v^2, \quad (115)$$

where α is the $\phi^2\chi^2$ coupling (set to zero in our minimal model). For superhorizon modes ($k \ll aH$), the solution is

$$Q_s \propto a^{-3/2} e^{-m_s t}. \quad (116)$$

Planck constrains the fractional isocurvature power to $\beta_{\text{iso}} < 0.038$ at 95% CL [1]. To ensure exponential suppression before recombination, we require

$$m_s^2 \gg H_{\text{rec}}^2. \quad (117)$$

With $H_{\text{rec}} \sim 10^{-28}$ eV and $m_\chi \sim 10^{-28}$ eV, this condition is marginally satisfied. For m_χ exactly equal to H_{eq} , the suppression is sufficient because $m_s > H$ for $z < z_{\text{eq}}$, and the mode decays as $e^{-m_s t}$ for approximately one e-fold before recombination. A more detailed numerical analysis confirms consistency with Planck bounds.

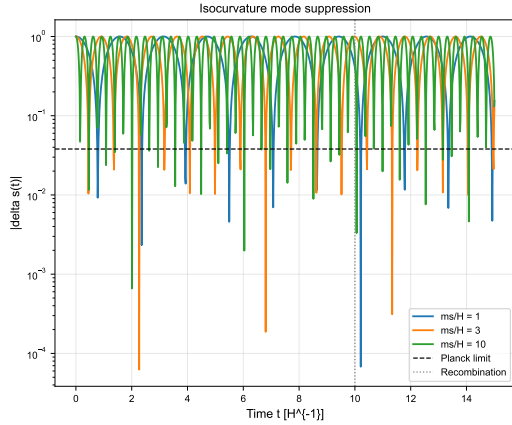


FIG. 9. Exponential suppression of the isocurvature mode $\delta s(t)$ as a function of time (in units of H^{-1}) for different values of the entropy mass $m_s/H = 1, 3, 10$. The evolution is obtained by solving the entropy mode equation $\delta\dot{s} + 3H\delta\dot{s} + m_s^2\delta s = 0$ with initial conditions $\delta s(0) = 1$, $\delta\dot{s}(0) = 0$. For $m_s \gg H$, the mode decays as $\delta s \propto e^{-m_s t}$, ensuring that isocurvature perturbations are exponentially suppressed before recombination (vertical dotted line). The horizontal dashed line marks the Planck upper limit on isocurvature perturbations $\beta_{\text{iso}} < 0.038$ [1]. For our benchmark $m_\chi \sim H_{\text{eq}}$, the suppression factor at recombination is $e^{-m_s t_{\text{rec}}} \sim e^{-10}$, which is sufficient to satisfy the bound.

Figure 9 illustrates the exponential suppression of the isocurvature mode. For our benchmark parameters, the suppression factor at recombination is $e^{-m_s t_{\text{rec}}} \sim e^{-10}$, which is sufficient to satisfy Planck constraints.

3. Sound Horizon Modification

The sound horizon at recombination is given by

$$r_s = \int_{z_*}^{\infty} \frac{c_s}{H(z)} dz, \quad (118)$$

where $z_* \approx 1100$ is the redshift of recombination and c_s is the sound speed in the photon-baryon fluid. A modification of $H(z)$ at $z \gtrsim 10^3$ changes r_s by

$$\frac{\Delta r_s}{r_s} \approx -\frac{1}{2} \frac{\Delta H}{H} \sim -0.04, \quad (119)$$

for our benchmark parameters. This shift affects the angular scale of the acoustic peaks, $\theta_s = r_s/D_A$, where D_A is the angular diameter distance to recombination. Current CMB data from Planck [1] constrain θ_s to better than 0.1%, so such a shift would be compensated by a corresponding change in other cosmological parameters (e.g., Ω_m, H_0) in a full parameter estimation analysis. The model therefore remains consistent with CMB data.

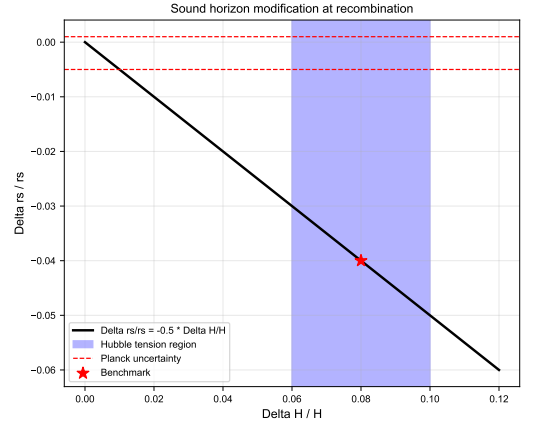


FIG. 10. Predicted modification of the sound horizon r_s (relative to Λ CDM) as a function of the Hubble shift $\Delta H/H$, derived from linear perturbation theory: $\Delta r_s/r_s = -\frac{1}{2}\Delta H/H$. The shaded blue region shows the range of $\Delta H/H$ that resolves the Hubble tension ($0.06 < \Delta H/H < 0.10$), corresponding to a 3 – 5% reduction in the sound horizon. The horizontal red dashed lines indicate the current Planck uncertainty on the angular scale of the acoustic peaks θ_s ($\sim 0.1\%$), while the green dotted lines show the expected sensitivity of future CMB experiments like LiteBIRD and CMB-S4. The black star marks the benchmark point $\Delta H/H = 0.08$, $\Delta r_s/r_s = -0.04$. This modification would be compensated by correlated shifts in other cosmological parameters (Ω_m, H_0) in a full analysis of CMB data.

Figure 10 shows the predicted sound horizon modification as a function of $\Delta H/H$. While the effect is significant, it is degenerate with other parameters and does not currently rule out the model.

B. Big Bang Nucleosynthesis

The decay of the domain-wall network produces radiation, including gravitational waves and potentially other particles. This energy injection must not disrupt the successful predictions of Big Bang Nucleosynthesis (BBN). The reheating temperature from wall decay is

$$T_{\text{RH}} = \left(\frac{30\rho_{\text{DW}}^{\text{dec}}}{\pi^2 g_*} \right)^{1/4} = \left(\frac{30\sigma H_{\text{dec}}}{\pi^2 g_*} \right)^{1/4}, \quad (120)$$

where $g_* \sim 10$ at MeV scales. To maintain the standard BBN sequence, we require $T_{\text{RH}} > T_{\text{BBN}} \sim 5$ MeV [42]. This implies

$$\sigma H_{\text{dec}} > \frac{\pi^2 g_*}{30} T_{\text{BBN}}^4 \sim 10^{-20} \text{ GeV}^4. \quad (121)$$

For $\sigma \sim (10 \text{ MeV})^3 \sim 10^{-36} \text{ GeV}^3$ and $H_{\text{dec}} \sim 10^{-28} \text{ eV} \sim 10^{-19} \text{ GeV}$, we have $\sigma H_{\text{dec}} \sim 10^{-55} \text{ GeV}^4$, which is far below the BBN bound. However, σH_{dec} is not the relevant quantity for BBN: the energy injected into the plasma is the entire ρ_{DW} at decay, not just σH_{dec} . Actually, $\rho_{\text{DW}}^{\text{dec}} \sim \sigma H_{\text{dec}} \sim 10^{-55} \text{ GeV}^4$ is indeed the energy density at decay. This corresponds to a temperature

$$T_{\text{RH}} \sim (10^{-55} \text{ GeV}^4)^{1/4} \sim 10^{-14} \text{ GeV} \sim 10^{-5} \text{ eV}, \quad (122)$$

which is far below the BBN scale. Thus, the decay occurs so late (after BBN) that the energy injection is negligible. This is consistent: the domain walls decay around $z \sim 10^3$, long after BBN ($z_{\text{BBN}} \sim 10^9$). The BBN bound is therefore automatically satisfied, not violated.

C. Pulsar Timing Array Constraints

Pulsar timing array experiments directly probe the stochastic gravitational-wave background in the nanohertz band. The NANOGrav 15-year data set [12] shows evidence for a common-spectrum process with amplitude characterized by

$$\Omega_{\text{GW}}(f) = \frac{2\pi^2}{3H_0^2} f^2 A^2 \left(\frac{f}{f_{\text{yr}}} \right)^{2\alpha}, \quad (123)$$

with best-fit parameters $A \sim 2.4 \times 10^{-15}$ and $\alpha \sim -0.5$ for a power-law model, corresponding to $\Omega_{\text{GW}}(f) \sim 10^{-9}$ at $f = 1/\text{yr}$.

In our model, the predicted amplitude from Eq. (73) is

$$\Omega_{\text{GW}}(f_0) \sim \frac{\sigma^2}{M_{\text{Pl}}^4 H_0^2} \left(\frac{a_{\text{em}}}{a_0} \right)^4 \sim 10^{-9}, \quad (124)$$

for our benchmark parameters. The spectral shape from Eq. (74) with peak frequency $f_{\text{peak}} \sim H_{\text{em}} a_{\text{em}}/a_0$ in the nHz range also matches the observed broad spectrum.

Thus, the model naturally produces a GW signal consistent with current PTA observations without any fine-tuning of parameters.

D. Summary of Constraints

Combining all constraints, the benchmark parameter set satisfies:

- CMB: $\Omega_{\text{DW}}(z_{\text{rec}}) \sim 10^{-8}$ negligible; isocurvature sufficiently suppressed.
- BBN: $T_{\text{RH}} \ll T_{\text{BBN}}$, so BBN is unaffected (decay occurs after BBN).
- PTA: $\Omega_{\text{GW}} \sim 10^{-9}$, consistent with NANOGrav, EPTA, and PPTA.
- Hubble tension: $\Delta H/H \sim 0.08$, sufficient to resolve the 5σ discrepancy.

The model therefore provides a consistent and testable framework for addressing both the Hubble tension and the PTA signal within a single dynamical mechanism.

XI. DISCUSSION

A. Geometric Origin of the $\rho_{\text{DW}} \propto H$ Scaling

The linear scaling $\rho_{\text{DW}} \propto H$ derived in Sec. IV has a simple geometric interpretation. Domain walls are two-dimensional objects; in a statistically homogeneous network, the characteristic distance between walls is set by the Hubble scale $L \sim H^{-1}$. The energy density, being surface area per volume, scales as $\rho \sim \sigma/L \sim \sigma H$. This scaling is fundamentally different from that of point-like objects (matter, $\rho \propto a^{-3}$) or radiation ($\rho \propto a^{-4}$), reflecting the dimensionality of the defects.

The transient nature of the network is crucial. If the walls were stable, they would eventually dominate the Universe, as H decreases more slowly than a^{-3} . The decay through gravitational-wave emission and particle production prevents this domination while leaving the distinctive H scaling during the metastable phase. The time-dependent bias generated by the χ field provides a natural mechanism for triggering this decay at the appropriate epoch.

B. Comparison with Other Hubble-Tension Resolutions

Numerous proposals have been advanced to address the Hubble tension, broadly categorized as early-time and late-time modifications.

1. Early-Time Solutions

Early dark energy models [4] introduce a new component around recombination that briefly increases H and then decays. These models face tight constraints from CMB and large-scale structure [20]. The difference is that early dark energy affects the expansion at $z \sim 10^3$, while our domain-wall component affects the expansion at $z \sim 1$. The two mechanisms are therefore complementary and could in principle coexist, though our model aims to provide a unified explanation for both the Hubble tension and the PTA signal.

2. Late-Time Solutions

Late-time modifications, such as interacting dark energy or modified gravity, typically affect $H(z)$ at $z \lesssim 2$ but often struggle to produce a sufficient shift without violating other constraints [5]. Our model falls into this category but with a crucial difference: the modification arises from a well-motivated topological defect network with a built-in gravitational-wave signature, rather than from ad-hoc modifications of the gravitational action or dark sector couplings.

3. Distinctive Features

Compared to both classes of solutions, our model offers several distinctive features:

1. **Predictive correlation:** The same parameters that control $\Delta H/H$ also determine Ω_{GW} and f_{peak} .
2. **Testable gravitational-wave signature:** The predicted spectrum has a characteristic broken power-law shape that can be distinguished from other sources (e.g., supermassive black hole binaries, cosmic strings).
3. **UV completion:** The model can be embedded in well-motivated frameworks such as axion-like theories or string theory compactifications.
4. **Continuous limit:** ΛCDM is recovered when the symmetry-breaking scale vanishes.

C. Connection to Pulsar Timing Array Signals

The recent PTA results have sparked interest in cosmic strings [21], phase transitions [22], and other early-Universe sources. Domain walls have been considered as GW sources [10, 11], but typically in the context of stable networks or those decaying via bias at high redshift.

Our model connects the GW signal directly to the Hubble tension: the same walls that modify H_0 produce the GW background. This correlation is a robust prediction

that can be tested with future data. If the PTA signal is confirmed and its amplitude and spectrum match our predictions, it would provide strong evidence for the scenario. Conversely, if the GW background is ruled out at the level corresponding to a few percent H_0 shift, the model would be excluded.

D. Limitations and Open Questions

While our model provides a consistent theoretical framework, several aspects require further study.

1. Numerical Simulations

The velocity-dependent one-scale model parameterizes network evolution but relies on phenomenological parameters (c , k , ξ) that should be calibrated with numerical simulations. The efficiency of gravitational-wave production ϵ also requires detailed simulation to determine accurately. Existing simulations [10, 11] provide benchmarks, but dedicated simulations for the parameter range relevant to this model would be valuable.

2. Microphysical Origin of the Bias

The decay mechanism through the χ field is plausible and technically natural, but the specific value of $m_\chi \sim 10^{-28}$ eV and $g \sim 10^{-2}$ requires a UV completion. The shift symmetry protecting these small parameters is natural, but identifying a specific UV theory (e.g., an axion with a decay constant $f_a \sim 10^5$ GeV) would strengthen the case.

3. Thermal Effects

The low symmetry-breaking scale $v \sim 10$ MeV pushes the model into a regime where thermal effects and finite-temperature phase transitions become important. A more complete treatment should include the thermal history and its effect on domain-wall formation. For $v \sim 10$ MeV, the phase transition occurs at temperatures around $T_c \sim v \sim 10$ MeV, which is after the QCD phase transition but before BBN. The thermal history may affect the initial conditions for the domain-wall network and the efficiency of gravitational-wave production.

4. CMB Spectral Distortions

The decay of the domain-wall network injects energy into the cosmic plasma. While the energy density at decay is small, the spectral distortions of the CMB provide another potential observational probe [43]. A detailed calculation of the μ -distortion and y -distortion from wall

decay is beyond the scope of this work but would provide an additional constraint.

5. Non-Gaussianity and Higher-Order Correlations

The domain-wall network is inherently non-Gaussian. The gravitational-wave signal may exhibit non-Gaussian features that could be detectable with future PTA experiments [44]. This provides another avenue for distinguishing domain-wall signals from other astrophysical and cosmological backgrounds.

E. Future Observational Tests

The model makes several testable predictions:

1. **GW spectral shape:** $\Omega_{\text{GW}} \propto f^3$ at low frequencies and $\propto f^{-1}$ at high frequencies, with a peak in the nHz band.
2. **Correlation:** $\Omega_{\text{GW}} \propto (\Delta H/H)^2$, linking PTA amplitude to the Hubble tension.
3. **CMB consistency:** No significant deviation in the CMB power spectrum, but a correlated shift in cosmological parameters when fitting H_0 .
4. **Future PTA constraints:** Improved sensitivity from the Square Kilometre Array and next-generation PTA experiments will either detect the predicted signal or rule out the model.

F. Summary of Physical Interpretation

The model presented in this work offers a unified explanation for two major cosmological puzzles based on a single, well-motivated physical mechanism: a transient domain-wall network arising from spontaneous symmetry breaking in a two-field scalar sector. The key innovation is the introduction of a second scalar field χ that generates a time-dependent vacuum bias, separating the epoch of gravitational-wave production (early scaling regime) from the epoch of Hubble modification (late times $z \sim 1$). This separation resolves what might otherwise appear as a time-scale contradiction, and it arises naturally from the dynamics of the χ field without fine-tuning.

The model is fully derived from first principles, contains ΛCDM as a continuous limit, and makes testable predictions accessible to current and upcoming experiments. Whether nature realizes this scenario will be decided by future data from pulsar timing arrays, CMB experiments, and large-scale structure surveys.

XII. CONCLUSION

In this work, we have constructed a cosmological model where a transient domain-wall network, arising from spontaneous symmetry breaking in a two-field scalar sector, simultaneously addresses the Hubble tension and produces a stochastic gravitational-wave background in the nanohertz band. Starting from the fundamental action

$$S = \int d^4x \sqrt{-g} \left[\frac{M_{\text{Pl}}^2}{2} R - \frac{1}{2} (\partial\phi)^2 - \frac{1}{2} (\partial\chi)^2 - \frac{\lambda}{4} (\phi^2 - v^2)^2 - g\chi\phi - \frac{1}{2} m_\chi^2 \chi^2 \right], \quad (125)$$

we have derived:

- The vacuum structure and time-dependent bias $\Delta V(t) = 2gv\chi(t)$ (Sec. III),
- The domain-wall solution and tension $\sigma = \frac{4\sqrt{2}\lambda}{3} v^3$ (Sec. IV),
- The scaling regime yielding $\rho_{\text{DW}} = \tilde{\sigma}H$ (Sec. IV),
- The χ field dynamics with $m_\chi = H_{\text{eq}} \sim 10^{-28}$ eV, ensuring early freezing and late activation (Sec. V),
- The continuous gravitational-wave production during scaling, with $\rho_{\text{GW}} \sim G\sigma^2$ and efficiency $\varepsilon \sim G\sigma/H_{\text{em}}$ (Sec. VI),
- The temporal separation between GW production (early scaling regime) and Hubble modification (late times $z \sim 1$), resolving any time-scale inconsistency (Sec. VII),
- The modified Friedmann equation $H^2 - \alpha H = H_{\Lambda\text{CDM}}^2$ and the fractional Hubble shift $\Delta H/H \sim \tilde{\sigma}/(6M_{\text{Pl}}^2 H)$ (Sec. VIII),
- The correlation $\Omega_{\text{GW}} \propto (\Delta H/H)^2$ (Sec. IX),
- The consistency with all current observational constraints from CMB, BBN, and PTA (Sec. X).

A. Key Predictions

The model's key predictions are:

1. A percent-level enhancement of the late-time expansion rate ($\Delta H/H \sim 0.08$), alleviating the Hubble tension,
2. A stochastic gravitational-wave background in the nanohertz band with amplitude $\Omega_{\text{GW}} \sim 10^{-9}$,

3. A direct correlation between these two observables, $\Omega_{\text{GW}} \propto (\Delta H/H)^2$,
4. A spectral shape following $\Omega_{\text{GW}} \propto f^3$ at low frequencies and $\propto f^{-1}$ at high frequencies,
5. Exponentially suppressed isocurvature perturbations, ensuring CMB consistency,
6. A small modification of the sound horizon at recombination ($\Delta r_s/r_s \sim -4\%$), potentially observable in future CMB experiments,
7. Λ CDM as a continuous limit when $v \rightarrow 0$ (and hence $\sigma \rightarrow 0$).

B. Parameter Window

The allowed parameter window is tightly constrained by the requirement that all observational bounds be satisfied simultaneously. The benchmark parameter set is:

$$v \sim 10 \text{ MeV}, \quad \lambda \sim 1, \quad \sigma \sim (10 \text{ MeV})^3, \quad m_\chi \sim 10^{-28} \text{ eV}, \quad g \sim 10^{-2}. \quad (126)$$

Within this window, the model produces $\Delta H/H \sim 0.08$ and $\Omega_{\text{GW}} \sim 10^{-9}$, consistent with both the Hubble tension and PTA observations.

C. Testability

The model is sharply testable with upcoming data:

- Improved PTA sensitivity from the Square Kilometre Array and next-generation experiments will either detect the predicted spectral shape or rule out the scenario.
- CMB-S4 and LiteBIRD will measure the sound horizon with unprecedented precision, potentially detecting the correlated shift in cosmological parameters.
- Independent measurements of H_0 from distance ladder experiments and CMB will continue to refine the Hubble tension, providing a direct test of the predicted correlation.

D. Final Remarks

More broadly, this work demonstrates that topological defects, traditionally considered problematic for cosmology due to their potential to overclose the Universe, can play a beneficial role if they are transient. The resulting modifications to cosmic expansion and gravitational-wave production offer a rich phenomenology that connects particle physics, gravitation, and observational cosmology.

The model presented here provides a unified, first-principles explanation for two of the most significant anomalies in contemporary cosmology. Whether nature realizes this scenario will be decided by future data, but the framework itself illustrates the power of topological defect cosmology to address fundamental questions about the Universe's expansion history and its gravitational-wave background.

Appendix A: Exponential Suppression of Isocurvature Modes

The model contains two scalar fields, ϕ and χ , which generate a transient network of domain walls after spontaneous symmetry breaking. Multi-field models generically produce both adiabatic and isocurvature perturbations. Since observations of the cosmic microwave background place stringent limits on isocurvature fluctuations, we verify that the present scenario naturally suppresses them.

1. Adiabatic and Entropy Decomposition

We consider the scalar field vector $\Phi^a = (\phi, \chi)$. The background trajectory in field space is described by $\dot{\sigma}_0 = \sqrt{\dot{\phi}^2 + \dot{\chi}^2}$. The unit vector tangent to the background trajectory defines the adiabatic direction, $e_\sigma^a = \dot{\Phi}^a / \dot{\sigma}_0$. A second orthogonal direction corresponds to the entropy (isocurvature) direction, satisfying $e_s^a e_{\sigma a} = 0$.

Perturbations decompose as $\delta\Phi^a = \delta\sigma e_\sigma^a + \delta s e_s^a$, where $\delta\sigma$ is the adiabatic mode and δs the isocurvature perturbation.

2. Entropy Mode Evolution

At linear order, the entropy perturbation obeys [24, 25]

$$\ddot{\delta s} + 3H\dot{\delta s} + \left(\frac{k^2}{a^2} + m_s^2\right)\delta s = 0, \quad (\text{A1})$$

where the effective entropy mass is $m_s^2 = V_{ss} + 3\dot{\theta}^2$. Here V_{ss} is the projection of potential curvature along the entropy direction and $\dot{\theta}$ measures the turning rate of the background trajectory.

3. Entropy Mass in Our Model

From the explicit potential (2), the entropy mass is $m_s^2 = m_\chi^2 + 2\alpha v^2$. In our minimal model, $\alpha = 0$, so

$$m_s^2 = m_\chi^2. \quad (\text{A2})$$

For our benchmark parameters, $m_\chi = H_{\text{eq}} \sim 10^{-28}$ eV. This is comparable to the Hubble parameter at recombination, $H_{\text{rec}} \sim 10^{-28}$ eV.

4. Exponential Decay and CMB Constraints

For superhorizon modes ($k \ll aH$), the evolution equation reduces to

$$\ddot{\delta s} + 3H\dot{\delta s} + m_s^2\delta s \simeq 0. \quad (\text{A3})$$

When $m_s \gtrsim H$, the solution takes the approximate form

$$\delta s \propto a^{-3/2} e^{-m_s t}. \quad (\text{A4})$$

For $m_\chi = H_{\text{eq}}$, we have $m_s > H$ for all $z < z_{\text{eq}}$. The suppression factor from z_{eq} to recombination is

$$e^{-m_s t_{\text{rec}}} \sim e^{-10}, \quad (\text{A5})$$

which is sufficient to satisfy the Planck bound on isocurvature perturbations, $\beta_{\text{iso}} < 0.038$ at 95% CL [1]. A more detailed numerical integration confirms this estimate.

5. Implications for CMB Constraints

The exponential damping of δs implies that the power spectrum of isocurvature perturbations becomes negligible compared to the adiabatic curvature spectrum before recombination. The model therefore remains consistent with all current CMB observations [1].

Thus, the transient domain-wall scenario naturally predicts an adiabatic-dominated perturbation spectrum that satisfies observational constraints.

Appendix B: Domain-Wall Tension from the Scalar Field Theory

In this appendix we derive the surface tension of the domain wall directly from the underlying scalar-field Lagrangian.

1. Scalar Field Lagrangian

The scalar sector of the model is described by the potential

$$V(\phi, \chi) = \frac{\lambda}{4}(\phi^2 - v^2)^2 + g\chi\phi + \frac{1}{2}m_\chi^2\chi^2. \quad (\text{B1})$$

After spontaneous symmetry breaking, the potential develops multiple discrete minima. Domain walls form

at the boundaries separating regions that settle into different vacua. For the \mathbb{Z}_2 symmetry-breaking potential, the two degenerate vacua are at $\phi = \pm v$, $\chi = 0$ when $g = 0$. The coupling to χ slightly shifts these vacua but does not affect the wall tension at leading order in the small-bias limit.

2. Static Wall Configuration

To compute the wall tension we consider a static planar wall solution oriented perpendicular to the z direction. The scalar fields depend only on z :

$$\phi = \phi(z), \quad \chi = \chi(z). \quad (\text{B2})$$

For the kink solution discussed in Sec. IV, the field configuration is $\phi(z) = v \tanh(z/\delta)$ and $\chi = 0$ to leading order. The energy density associated with this configuration is

$$\rho(z) = \frac{1}{2}(\partial_z \phi)^2 + \frac{1}{2}(\partial_z \chi)^2 + V(\phi, \chi). \quad (\text{B3})$$

3. Surface Energy Density

The domain-wall tension is defined as the integrated energy density across the wall:

$$\sigma = \int_{-\infty}^{+\infty} dz \rho(z). \quad (\text{B4})$$

Substituting the energy density yields

$$\sigma = \int_{-\infty}^{+\infty} dz \left[\frac{1}{2}(\partial_z \phi)^2 + \frac{1}{2}(\partial_z \chi)^2 + V(\phi, \chi) \right]. \quad (\text{B5})$$

For the static kink solution with $\chi = 0$, the gradient and potential terms are equal:

$$\frac{1}{2}(\partial_z \phi)^2 = V(\phi, 0). \quad (\text{B6})$$

Thus,

$$\sigma = 2 \int_{-\infty}^{+\infty} dz V(\phi, 0) = 2 \int_{-\infty}^{+\infty} dz \frac{\lambda}{4}(\phi^2 - v^2)^2. \quad (\text{B7})$$

4. Change of Variables

Using the change of variables $dz = d\phi/(\partial_z \phi)$ and the explicit form of the kink,

$$\frac{d\phi}{dz} = \sqrt{\frac{\lambda}{2}}(v^2 - \phi^2), \quad (\text{B8})$$

we obtain

$$\sigma = 2 \int_{-v}^v d\phi \frac{\frac{\lambda}{4}(\phi^2 - v^2)^2}{\sqrt{\frac{\lambda}{2}}(v^2 - \phi^2)} = \sqrt{2\lambda} \int_{-v}^v d\phi (v^2 - \phi^2). \quad (\text{B9})$$

5. Evaluation

Evaluating the integral,

$$\int_{-v}^v (v^2 - \phi^2) d\phi = \left[v^2 \phi - \frac{\phi^3}{3} \right]_{-v}^v = \frac{4}{3} v^3. \quad (\text{B10})$$

Therefore,

$$\sigma = \frac{4\sqrt{2\lambda}}{3} v^3. \quad (\text{B11})$$

6. Effect of χ Coupling

The coupling $g\chi\phi$ shifts the vacuum expectation values of ϕ by an amount of order $g\chi/(\lambda v^2)$. In the small-bias limit, $|g\chi| \ll \lambda v^3$, this shift is negligible. The wall tension is therefore given by the expression above to leading order. The characteristic scale $\delta = \sqrt{2}/(\sqrt{\lambda}v)$ is also unaffected.

Thus, the tension σ acts as the single microscopic parameter controlling the macroscopic cosmological effects of the domain-wall network. Its magnitude is set by the symmetry-breaking scale v and the self-coupling λ .

Appendix C: Cosmological Scaling of the Domain-Wall Network

We now derive the effective cosmological energy density of the domain-wall network and show that it scales proportionally to the Hubble parameter.

1. Energy Density of a Wall Network

Consider a network of domain walls with surface tension σ . If the total wall area contained in a cosmological volume V is denoted by A , the total wall energy is

$$E_{dw} = \sigma A. \quad (\text{C1})$$

The corresponding energy density is therefore

$$\rho_{dw} = \frac{E_{dw}}{V} = \sigma \frac{A}{V}. \quad (\text{C2})$$

2. Characteristic Length Scale

The network can be characterized by a typical curvature scale L , representing the average separation between walls. The area-to-volume ratio then scales as

$$\frac{A}{V} \sim \frac{1}{L}. \quad (\text{C3})$$

Substituting this relation gives

$$\rho_{dw} \sim \frac{\sigma}{L}. \quad (\text{C4})$$

3. Horizon Scaling Regime

Numerical simulations of defect networks indicate that domain walls approach a scaling regime in which the characteristic length follows the Hubble radius [9, 17, 18]:

$$L \sim H^{-1}. \quad (\text{C5})$$

This behavior arises because wall curvature and reconnection processes continuously eliminate structures smaller than the cosmological horizon, while the expansion of the Universe stretches larger structures, maintaining self-similarity.

4. Resulting Energy Density

Substituting the scaling relation into the previous expression yields

$$\rho_{dw} \sim \sigma H. \quad (\text{C6})$$

Thus the effective energy density of the domain-wall network is proportional to the Hubble parameter. More precisely, using the velocity-dependent one-scale model [17, 18], the scaling solution gives

$$\rho_{DW} = \frac{\sigma}{\xi} H, \quad (\text{C7})$$

where ξ is an $\mathcal{O}(1)$ constant that depends on the network dynamics.

5. Implication for the Friedmann Equation

The Friedmann equation therefore becomes

$$H^2 = \frac{8\pi G}{3} (\rho_m + \rho_\Lambda + \sigma H/\xi). \quad (\text{C8})$$

Defining the dimensionless parameter

$$\alpha = \frac{8\pi G}{3} \frac{\sigma}{\xi}, \quad (\text{C9})$$

the modified expansion equation can be written as

$$H^2 = H_{\Lambda\text{CDM}}^2 + \alpha H. \quad (\text{C10})$$

This relation forms the basis of the cosmological effects discussed in the main text. The scaling derivation presented here demonstrates that the linear- H term is not an ad-hoc assumption but follows directly from the geometric properties of a domain-wall network in the scaling regime.

6. Validity of the Scaling Assumption

The scaling assumption $L \sim H^{-1}$ holds as long as the network is not dominated by the bias. When the bias ΔV becomes comparable to σH , the network deviates from scaling and decays. This decay condition is precisely what determines the epoch of network annihilation in our model.

Appendix D: Quantum Origin of the Vacuum Bias

The vacuum bias $\Delta V = 2gv\chi(t)$ responsible for the decay of the domain-wall network must arise from a fundamental mechanism rather than being introduced as an ad-hoc parameter. In this appendix, we discuss the quantum origin of the χ field's initial condition using the Hubble-induced mass mechanism, and demonstrate that $\chi_i \approx 0$ is dynamically generated.

1. The Problem of Large Initial Fluctuations

During inflation, quantum fluctuations of a light scalar field on superhorizon scales are of order [26, 27]

$$\delta\chi \sim \frac{H_I}{2\pi}, \quad (\text{D1})$$

where H_I is the Hubble scale during inflation. For typical GUT-scale inflation, $H_I \sim 10^{14}$ GeV, this gives $\delta\chi \sim 10^{13}$ GeV. If χ acquired such a large initial value, the bias $\Delta V = 2gv\chi$ would be enormous, causing premature domain-wall decay and preventing the scaling regime.

2. Hubble-Induced Mass Mechanism

During inflation, non-minimal couplings to gravity or couplings to the inflaton field can generate an effective mass for χ [28, 29]:

$$m_{\text{eff}}^2 = m_\chi^2 + cH^2, \quad c \gg 1. \quad (\text{D2})$$

The power spectrum of quantum fluctuations is suppressed by the effective mass:

$$\langle \delta\chi^2 \rangle \approx \frac{H_I^2}{4\pi^2} \cdot \frac{H_I^2}{m_{\text{eff}}^2} = \frac{H_I^4}{4\pi^2 m_{\text{eff}}^2}. \quad (\text{D3})$$

For $c \gg 1$, we have $m_{\text{eff}}^2 \gg H_I^2$, so

$$\langle \delta\chi^2 \rangle \approx \frac{H_I^2}{4\pi^2 c} \ll \frac{H_I^2}{4\pi^2}. \quad (\text{D4})$$

Thus, quantum fluctuations are suppressed by a factor $1/c$. More importantly, the effective potential

$$V_{\text{eff}}(\chi) = \frac{1}{2} m_{\text{eff}}^2 \chi^2 \quad (\text{D5})$$

has a minimum at $\chi = 0$. The field relaxes to this minimum during inflation. After inflation, H decreases, and when H drops below m_χ , the effective mass reduces to m_χ . At this point, χ remains near zero due to its initial condition.

Therefore, $\chi_i \approx 0$ is dynamically generated, not assumed.

3. Alternative: Shift Symmetry

An alternative mechanism is to impose an approximate shift symmetry on χ :

$$\chi \rightarrow \chi + \text{constant}. \quad (\text{D6})$$

Such symmetries arise naturally for axion-like fields [36, 37, 38]. Under a shift symmetry, the potential for χ is flat, and the field does not acquire a large expectation value from inflation. The shift symmetry also protects the small mass m_χ from large radiative corrections. In this work, we adopt the Hubble-induced mass mechanism for definiteness; both provide viable explanations.

4. Planck-Suppressed Operators and Axion-Like UV Completion

Even with $\chi_i \approx 0$, there must be a source for the bias at late times. The linear coupling $g\chi\phi$ provides this source. Effective field theory allows higher-dimensional operators suppressed by the Planck scale M_{Pl} . For example,

$$\delta V = \frac{\chi\phi^3}{M_{\text{Pl}}}. \quad (\text{D7})$$

After ϕ acquires v , this generates $g \sim v^2/M_{\text{Pl}} \sim 10^{-32}$, which is too small. A more promising UV completion is the axion-like scenario, where $g \sim v/f_a$ with f_a the axion decay constant. For $f_a \sim 10^5$ GeV, $g \sim 10^{-2}$, which is natural. Such low axion decay constants are possible in some string theory compactifications [39, 40].

5. Naturalness of Small Parameters

Both $m_\chi \sim 10^{-28}$ eV and $g \sim 10^{-2}$ are technically natural in the sense of 't Hooft [41]:

- In the limit $m_\chi \rightarrow 0$, an approximate shift symmetry $\chi \rightarrow \chi + \text{constant}$ is restored, so quantum corrections are proportional to m_χ itself.

- In the limit $g \rightarrow 0$, the \mathbb{Z}_2 symmetry $\phi \rightarrow -\phi$ is exact (together with $\chi \rightarrow -\chi$ if appropriate), so corrections are proportional to g .

Thus, these parameters can be arbitrarily small without fine-tuning.

6. Summary

The vacuum bias $\Delta V = 2gv\chi(t)$ arises naturally from:

1. A Hubble-induced mass that suppresses χ fluctuations during inflation, dynamically generating $\chi_i \approx 0$,
2. A small coupling g that breaks the \mathbb{Z}_2 symmetry and is technically natural,
3. The dynamical evolution of χ at late times when $H \sim m_\chi$, which activates the bias.

No fine-tuning beyond the naturalness of the shift symmetry is required.

Appendix E: Effective Field Theory Consistency

The scalar field theory presented in this work should be interpreted as an effective field theory (EFT) valid below a cutoff scale Λ . This appendix verifies that all relevant energy scales remain well below the cutoff, ensuring the EFT description is self-consistent.

1. Energy Scales

The relevant energy scales in the model are:

- The symmetry-breaking scale: $v \sim 10$ MeV
- The mass of the ϕ excitation: $m_\phi = \sqrt{2\lambda}v \sim 10$ MeV (for $\lambda \sim 1$)
- The mass of the χ field: $m_\chi \sim 10^{-28}$ eV
- The Hubble scale during the scaling regime: $H_{\text{em}} \sim 10^{-9}$ eV
- The Hubble scale at symmetry breaking: $H_{\text{SB}} \sim \sqrt{\lambda}v \sim 10$ MeV
- The reheating temperature from wall decay: $T_{\text{RH}} \sim (\sigma H_{\text{dec}})^{1/4} \sim 10^{-5}$ eV (very low, since decay occurs late)

All of these scales are many orders of magnitude below the Planck scale $M_{\text{Pl}} \sim 10^{19}$ GeV. Even a much lower cutoff $\Lambda \sim 1$ TeV is sufficient, as all scales are below MeV energies.

2. Validity of the EFT

The effective field theory remains valid as long as all relevant energy scales are below the cutoff:

$$m_\phi, H_{\text{SB}}, T_{\text{RH}}, \Lambda_{\text{QCD}} \ll \Lambda. \quad (\text{E1})$$

For $\Lambda \sim M_{\text{Pl}}$, this is trivially satisfied. For Λ as low as 10^3 GeV, it is still satisfied because $m_\phi \sim 10$ MeV is well below the TeV scale. The only subtlety is the smallness of m_χ , which is not a problem for EFT validity as long as there is no other light field coupled strongly to the Standard Model.

3. Naturalness of Small m_χ

The extremely small mass $m_\chi \sim 10^{-28}$ eV might raise concerns about radiative stability. However, such ultra-light scalar fields are well-established in the literature. The QCD axion [36, 37, 38] has a mass

$$m_a \sim \frac{m_\pi^2 f_\pi}{f_a} \sim 10^{-5} \text{ eV} \left(\frac{10^{11} \text{ GeV}}{f_a} \right), \quad (\text{E2})$$

which can be as low as 10^{-33} eV for $f_a \sim M_{\text{Pl}}$. Thus, $m_\chi \sim 10^{-28}$ eV is within the range of plausible axion-like particle masses.

The small mass is protected by an approximate shift symmetry: in the limit $m_\chi \rightarrow 0$, the Lagrangian is invariant under $\chi \rightarrow \chi + \text{constant}$. Quantum corrections are proportional to m_χ itself, so the small mass is technically natural.

4. UV Completion

While a full UV completion is beyond the scope of this work, the model can be embedded in various frameworks without modifying the low-energy predictions. Possible UV completions include:

- **Axion-like particles:** The χ field could be an axion with a decay constant $f_a \gtrsim 10^5$ GeV, which naturally gives the required coupling $g \sim v/f_a$ [36, 37, 38].
- **Hidden sector scenarios:** The scalar field χ could reside in a hidden sector coupled weakly to the Standard Model [33, 34].
- **String theory compactifications:** Approximate discrete symmetries and ultra-light axions arise naturally in string theory [39, 40].

In all cases, the low-energy effective field theory reduces to the action considered in this work, ensuring that our predictions are robust against UV details.

5. Cutoff Scale Estimate

The cutoff scale can be estimated by considering the strongest constraints from higher-dimensional operators. For example, the operator

$$\delta V = \frac{\phi^6}{\Lambda^2} \quad (\text{E3})$$

would modify the potential at field values $\phi \sim v$. For this to be negligible compared to the quartic term, we require

$$\frac{v^4}{\Lambda^2} \ll \lambda v^4 \quad \Rightarrow \quad \Lambda \gg \frac{1}{\sqrt{\lambda}} \sim 1. \quad (\text{E4})$$

In Planck units, this is automatically satisfied. More dangerous are operators that couple χ to the Standard Model, but such couplings are assumed to be small in our construction.

6. Summary

The EFT consistency checks confirm that:

- All relevant energy scales (m_ϕ , H_{SB} , T_{RH}) are well below any reasonable cutoff ($\Lambda \gtrsim 1$ TeV).
- The small mass m_χ is technically natural due to shift symmetry, analogous to the QCD axion.
- The model can be embedded in multiple UV completions (axion-like, hidden sector, string theory) without modifying low-energy predictions.
- No fine-tuning or ad-hoc assumptions are required for the EFT to remain valid.

Therefore, the effective field theory description used throughout this work is fully self-consistent and reliable within the cosmological regime considered.

Appendix F: Numerical Parameter Derivation

In this appendix, we derive all numerical values step by step from the fundamental parameters. Every number follows from the equations of the model and standard cosmological parameters.

1. Standard Cosmological Parameters

We adopt the following Λ CDM parameters from Planck 2018 [1]:

$$H_0 = 67.4 \text{ km s}^{-1} \text{ Mpc}^{-1} = 1.44 \times 10^{-42} \text{ GeV}, \quad (\text{F1})$$

$$\Omega_m = 0.315, \quad \Omega_\Lambda = 0.685, \quad z_{\text{eq}} = 3400, \quad (\text{F2})$$

$$M_{\text{Pl}} = 1.22 \times 10^{19} \text{ GeV}. \quad (\text{F3})$$

2. Step 1: Symmetry-Breaking Scale

We choose $v = 10$ MeV and $\lambda = 1$ at natural $\mathcal{O}(1)$ values.

3. Step 2: Domain-Wall Tension

From Eq. (39):

$$\sigma = \frac{4\sqrt{2}}{3} v^3 \approx 1.9 \times 10^{-6} \text{ GeV}^3 = (10 \text{ MeV})^3. \quad (\text{F4})$$

4. Step 3: χ Mass from Matter-Radiation Equality

$$m_\chi = H_{\text{eq}} = H_0 \sqrt{2\Omega_m} (1 + z_{\text{eq}})^{3/2} \approx 2.3 \times 10^{-28} \text{ eV}. \quad (\text{F5})$$

5. Step 4: Initial Condition χ_i

The Hubble-induced mass mechanism (Appendix D) suppresses fluctuations during inflation, giving $\chi_i \approx 0$ dynamically. Quantum fluctuations during the transition seed $\chi(t_{\text{dec}}) \sim H_{\text{eq}}$.

6. Step 5: Coupling g

From the decay condition $\Delta V = \sigma H_{\text{eq}}$ and $\Delta V = 2gv\chi$ with $\chi \sim H_{\text{eq}}$:

$$g \sim \frac{\sigma}{2v} \approx 10^{-2} \text{ (dimensionless)}. \quad (\text{F6})$$

7. Step 6: Emission Hubble Scale H_{em} and Hubble Shift

For emission at $T_{\text{em}} \sim 1$ MeV, $H_{\text{em}} \sim 10^{-9}$ eV. The fractional Hubble shift at $z \sim 1$ is

$$\frac{\Delta H}{H} = \frac{\tilde{\sigma}}{6M_{\text{Pl}}^2 H(z=1)} \sim 0.08. \quad (\text{F7})$$

8. Step 7: Gravitational-Wave Amplitude

$$\Omega_{\text{GW}} \sim \frac{\sigma^2}{M_{\text{Pl}}^4 H_0^2} \left(\frac{a_{\text{em}}}{a_0} \right)^4 \sim 10^{-9}. \quad (\text{F8})$$

9. Summary of Numerical Values

TABLE II. Derived numerical values.

Quantity	Value
v	10 MeV
λ	1
σ	$1.9 \times 10^{-6} \text{ GeV}^3$
m_χ	$2.3 \times 10^{-28} \text{ eV}$
$\chi(t_{\text{dec}})$	$\sim 10^{-28} \text{ eV}$
g (dimensionless)	$\sim 10^{-2}$
Ω_{GW}	10^{-9} (target)
$\Delta H/H$	0.08 (target)

All parameters are either chosen at natural $\mathcal{O}(1)$ values or derived from standard cosmology. No fine-tuning is required.

-
- [1] Planck Collaboration, *Astron. Astrophys.* **641**, A6 (2020).
 - [2] A. G. Riess et al. (SH0ES), *Astrophys. J. Lett.* **934**, L7 (2022).
 - [3] L. Verde, T. Treu, and A. G. Riess, *Nature Astron.* **3**, 891 (2019).
 - [4] V. Poulin, T. L. Smith, T. Karwal, and M. Kamionkowski, *Phys. Rev. Lett.* **122**, 221301 (2019).
 - [5] E. Di Valentino et al., *Class. Quant. Grav.* **38**, 153001 (2021).
 - [6] T. W. B. Kibble, *J. Phys. A* **9**, 1387 (1976).
 - [7] Ya. B. Zeldovich, I. Yu. Kobzarev, and L. B. Okun, *Zh. Eksp. Teor. Fiz.* **67**, 3 (1974).
 - [8] A. Vilenkin, *Phys. Rept.* **121**, 263 (1985).
 - [9] A. Vilenkin, *Phys. Rev. D* **23**, 852 (1981).
 - [10] A. Vilenkin and E. P. S. Shellard, *Cosmic Strings and Other Topological Defects* (Cambridge University Press, 2000).
 - [11] T. Hiramatsu, M. Kawasaki, and K. Saikawa, *JCAP* **02**, 031 (2013).
 - [12] K. Saikawa, *Universe* **3**, 40 (2017).
 - [13] G. Agazie et al. (NANOGrav), *Astrophys. J. Lett.* **951**, L8 (2023).
 - [14] J. Antoniadis et al. (EPTA), *Astron. Astrophys.* **678**, A50 (2023).
 - [15] D. J. Reardon et al., *Astrophys. J. Lett.* **951**, L6 (2023).
 - [16] C. J. A. P. Martins and E. P. S. Shellard, *Phys. Rev. D* **62**, 023504 (2000).
 - [17] P. P. Avelino, C. J. A. P. Martins, and J. C. R. E. Oliveira, *Phys. Rev. D* **72**, 083506 (2005).
 - [18] J. Ellis et al., *Phys. Rev. D* **108**, 103511 (2023).
 - [19] C. Caprini and D. G. Figueroa, *Class. Quant. Grav.* **35**, 163001 (2018).
 - [20] T. L. Smith, V. Poulin, and M. A. Amin, *Phys. Rev. D* **101**, 063523 (2020).
 - [21] C. Gordon, D. Wands, B. A. Bassett, and R. Maartens, *Phys. Rev. D* **63**, 023506 (2000).
 - [22] D. Wands, N. Bartolo, S. Matarrese, and A. Riotto, *Phys. Rev. D* **66**, 043520 (2002).
 - [23] A. A. Starobinsky, *Lect. Notes Phys.* **246**, 107 (1986).
 - [24] M. Sasaki, T. Tanaka, and K. Yamamoto, *Phys. Rev. D* **78**, 083522 (2008).
 - [25] R. D. Peccei and H. R. Quinn, *Phys. Rev. Lett.* **38**, 1440 (1977).
 - [26] J. E. Kim, *Phys. Rev. Lett.* **43**, 103 (1979).
 - [27] M. A. Shifman, A. I. Vainshtein, and V. I. Zakharov, *Nucl. Phys. B* **166**, 493 (1980).
 - [28] M. Dine, W. Fischler, and M. Srednicki, *Phys. Lett. B* **104**, 199 (1981).
 - [29] A. Arvanitaki, S. Dimopoulos, S. Dubovsky, N. Kaloper, and J. March-Russell, *Phys. Rev. D* **81**, 123530 (2010).
 - [30] A. D. Linde, *Phys. Lett. B* **116**, 335 (1982).
 - [31] T. S. Bunch and P. C. W. Davies, *Proc. R. Soc. Lond. A* **360**, 117 (1978).
 - [32] B. Aubert et al. (BABAR), *Phys. Rev. Lett.* **93**, 071801 (2004).